AD-A103 481 ROCKWELL INTERNATIONAL THOUSAND OAKS CA MICROELECTR--ETC F/G 17/8
NOISE REDUCTION FOR FIBER OPTIC SENSORS.(U)
JUN 81 V VALI, M BERG N00173-80-C-0108
UNCLASSIFIED C80-380/501 NL

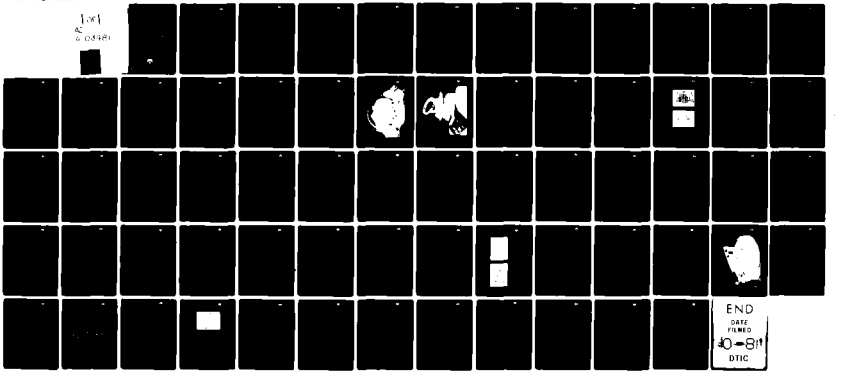

C80-380/501

NOISE REDUCTION FOR FIBER OPTIC SENSORS

FINAL REPORT FOR THE PERIOD
March 14, 1980 through January 14, 1981

GENERAL ORDER NO. 40301
CONTRACT NO. N00173-80-C-0108

Prepared for

Receiving Officer, Code N00173
Naval Research Laboratory
Washington, D.C. 20375
Non Milstrip

V. Vali and M. Berg

JUNE 1981

Rockwell International
Microelectronics Research and
Development Center

TABLE OF CONTENTS

LIST OF FIGURES

LIST OF FIGURES

LIST OF TABLES

INTRODUCTION AND SUMMARY

It is well established that interferometers with single-mode optical fibers as the propagation paths can be used as sensors for rotation rate,[1-6] acoustic pressure,[7-13] and magnetic field.[14,15] Calculations have indicated that some types of optical sensor, including fiber optic gyroscopes and hydrophones, have the potential for performing much better than conventional rotation rate and acoustic pressure sensors. However, these calculations assume that the noise is determined by statistical fluctuations in the photon emission rate, and the observed noise in fiber optic sensors in the laboratory has been an order of magnitude above this quantum noise limit. In order for practical fiber optic sensors to become a reality, it will be necessary to greatly reduce the noise contribution from effects other than the (fundamental) quantum fluctuations.

The causes for the fringe position uncertainty (the noise sources) are listed below in order of their importance.

1. Reflections in the system. To see other noises, reflections have to be eliminated. This is done using index matching fluids or appropriate angles on the optical parts.

2. Polarization caused nonreciprocity. This noise seems to be under control using polarization maintaining fibers.

3. Variable nonreciprocity caused by component motion. The proposed effort addresses this problem.

4. Core cladding interaction. It is necessary to continuously mode strip all along the fiber. This can be done by using PVC coating on the fiber instead of the RTV as presently used.

5. Temperature change and wavelength change of the light source change the scale factor of the gyroscope. Can probably be kept under 10^{-6} or better with not too much effort.

In order to place the projected fiber gyroscope performance the following six graphs were prepared Figs. 1 to 5). Here the minimum resolvable angular velocity is obtained from[1]

$$\delta(\omega) = \delta(\Delta Z)\,\frac{\lambda c}{2LR} \tag{1}$$

where $\delta(\Delta Z)$ is the fringe error (as caused by all the noise sources), λ is the wavelength of light, c is the velocity of light, L is the fiber length, and R is the fiber coil radius. The resolvable angular velocity is given as a function of the fiber length with the fringe position uncertainty as a parameter. This is done for fiber coil diameters from 5 cm to 1 meter. For easier comparison the minimum measurable (resolvable) angular velocity is given in degrees per hour.

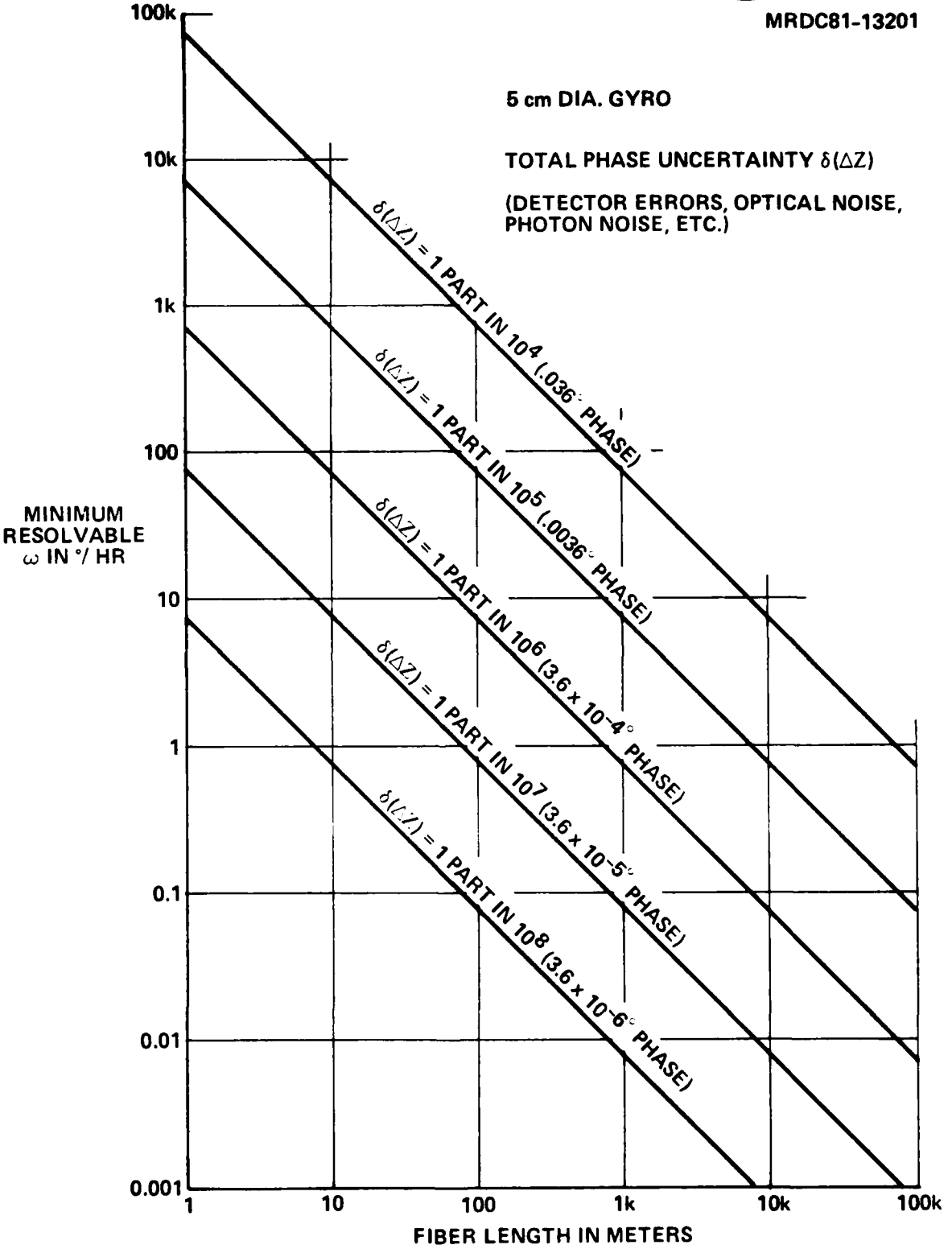

Fig. 1 5 cm dia. gyro.

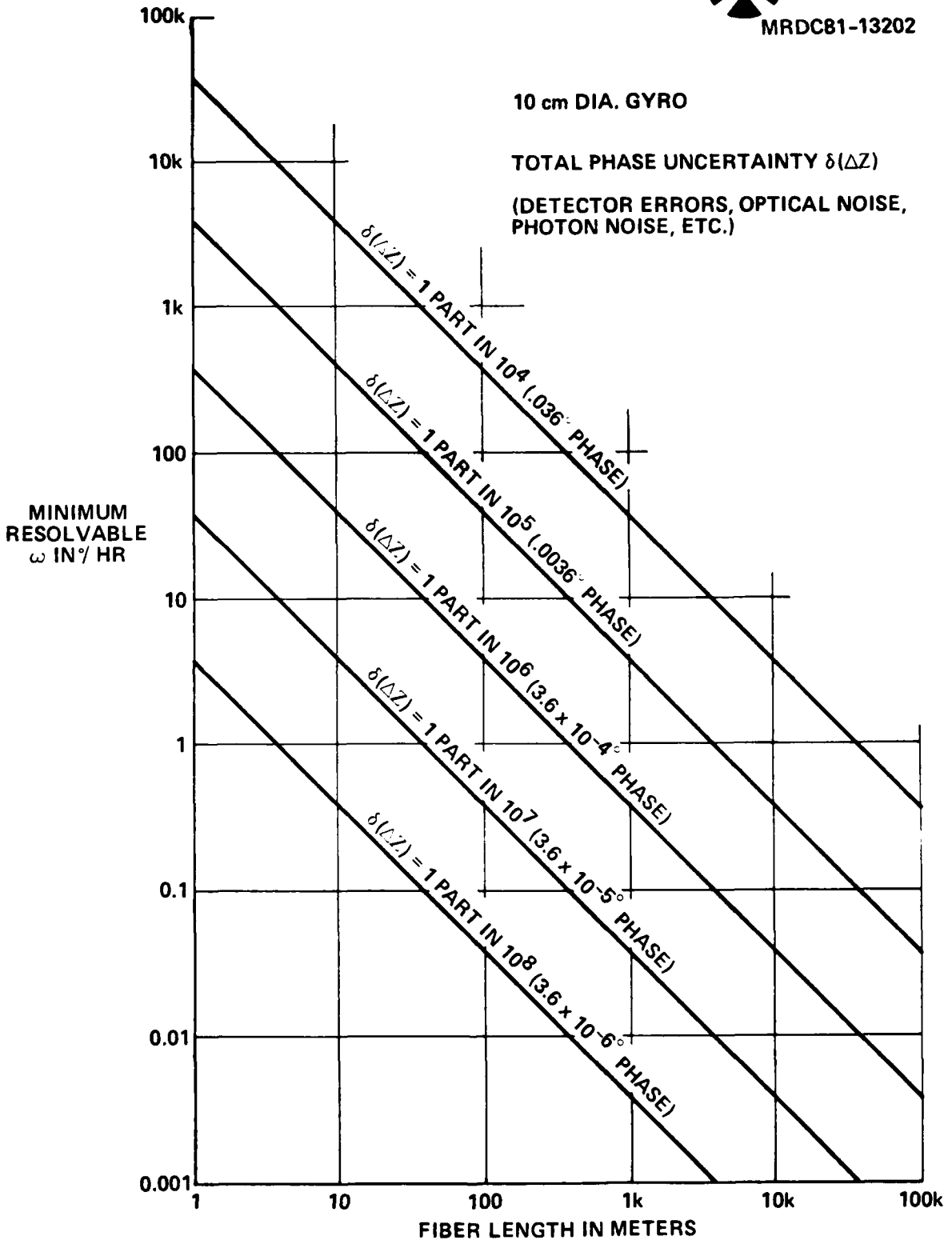

Fig. 2 10 cm dia. gyro.

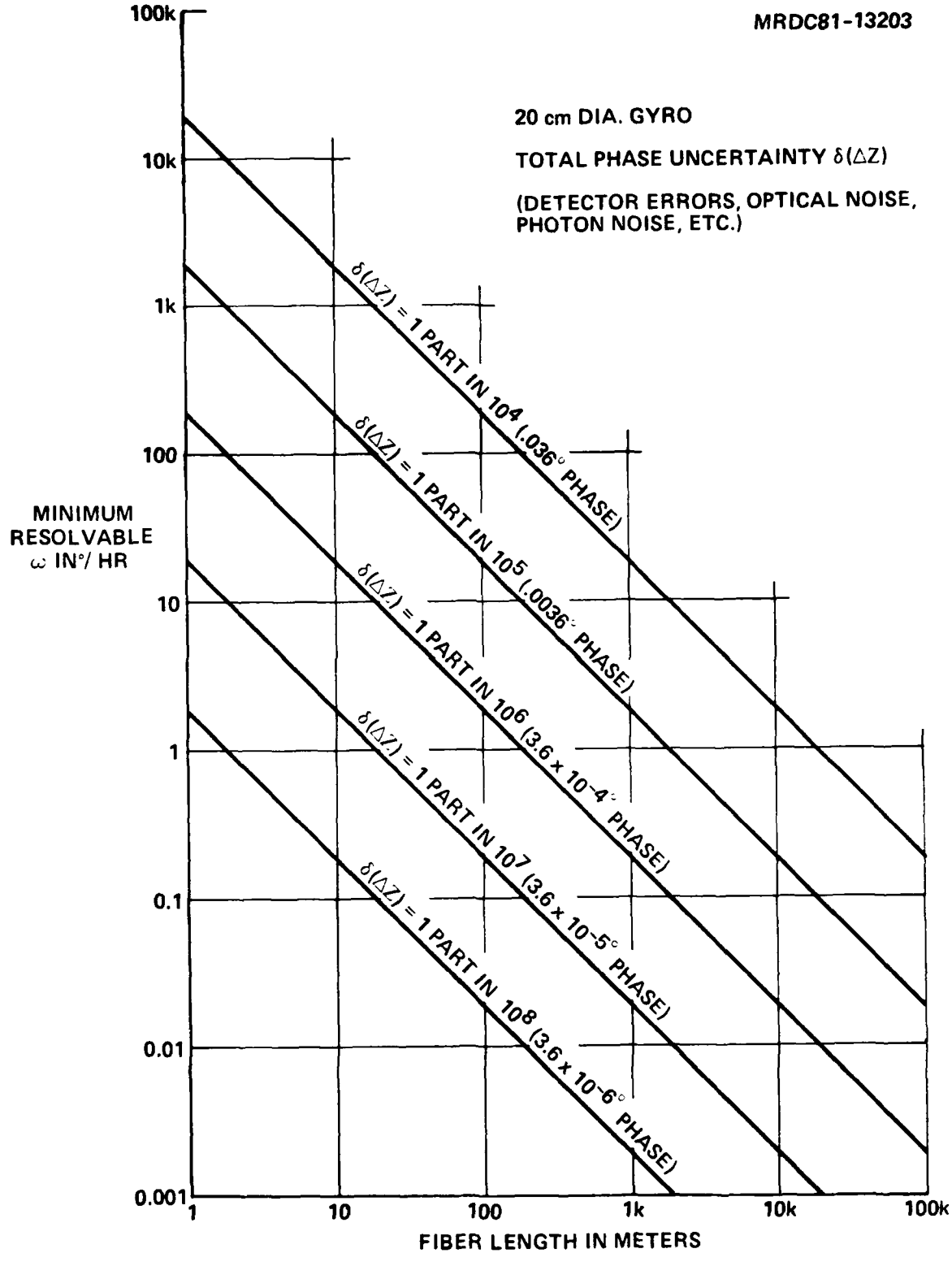

Fig. 3 20 cm dia. gyro.

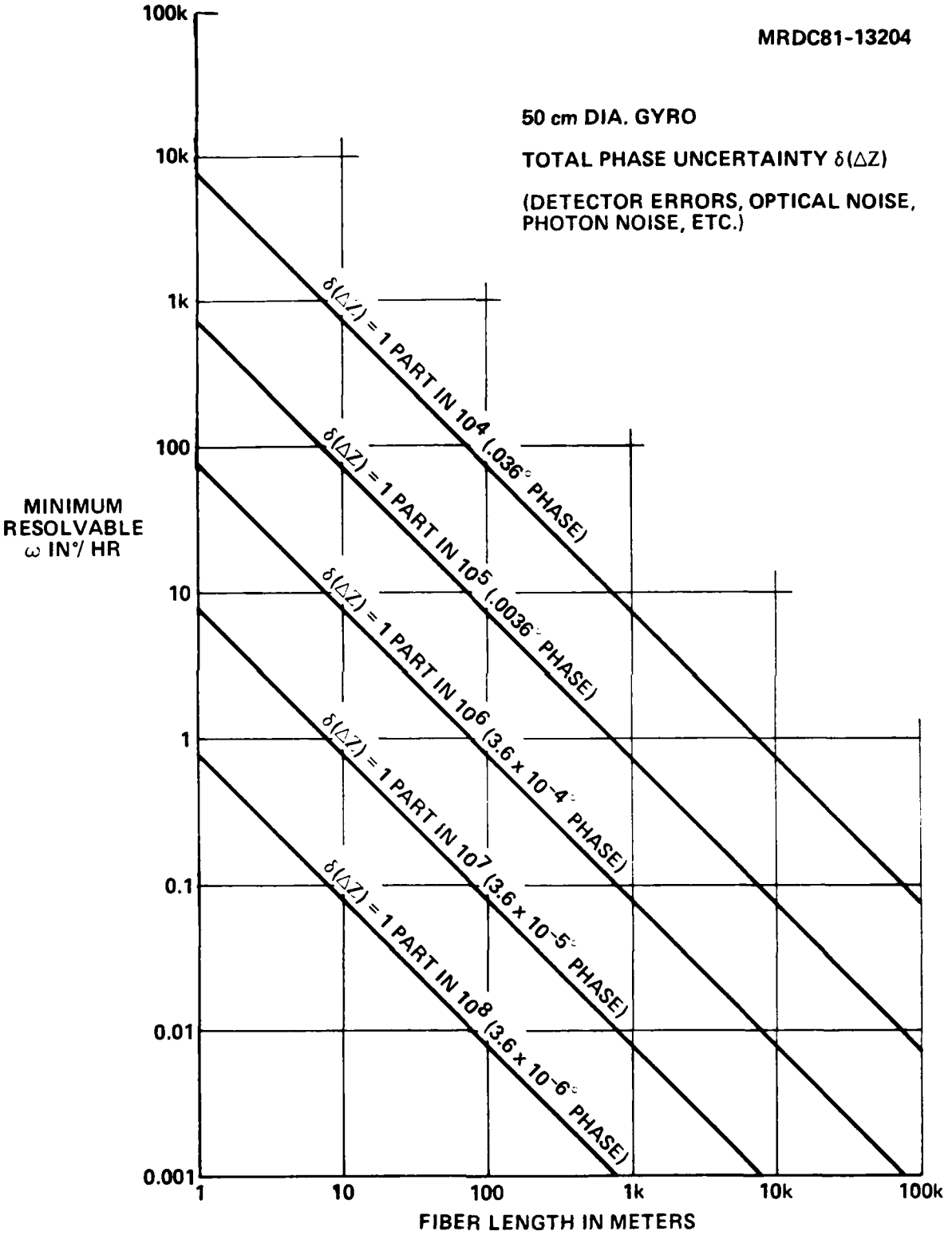

Fig. 4 50 cm dia. gyro.

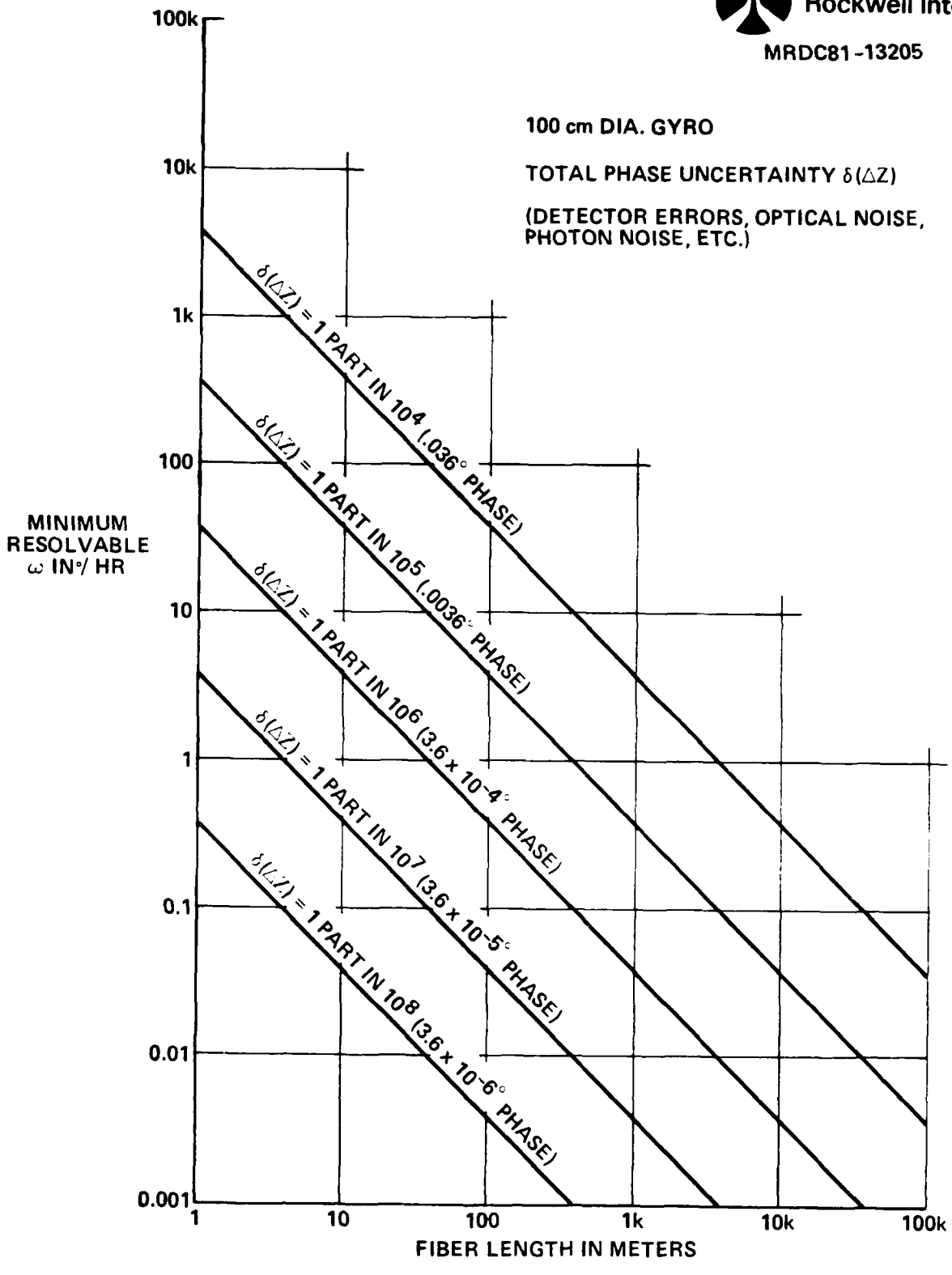

Fig. 5 100 cm dia. gyro.

In considering the noise in fiber optic sensors, it is useful to contrast the fiber optic gyro, which is based on the Sagnac interferometer, with the acoustic sensor based on the Mach-Zender configuration. Table I compares the influence of a number of potential noise sources on the performance of the two sensor types. As Table I indicates, several important noise effects are common, but the fact that the two beams traverse the same optical path in the Sagnac interferometer greatly reduces the susceptability of the gyro to most of the noise sources indicated. On the other hand, to be competitive with conventional inertial grade instruments the performance of the fiber optic gyro will have to approach to within a few dB of the quantum limit, while a noise level 10-20 dB above the quantum limit may be tolerable in some hydrophone applications. Futhermore, some problems such as the effect of coupling the interferometer output into the optical source and the necessity of producing a controllable and accurately measurable phase shift are peculiar to the Sagnac gyro.

Table I

Comparison of Noise Effects in the Fiber Optic Gyroscope and the Fiber Optic Hydrophone

	Noise Source	Sagnac Fiber Gyro	Fiber Hydrophone (Two Equal-Length Fibers)
1.	Reflections	Have to be eliminated to see other noises	Have to be eliminated to see other noises
2.	Polarization	Second order effect (only difference appears)	Effect much larger (two different fibers)
3.	Component Motion	Second order effect (only nonreciprocal difference appears)	First order effect
4.	Core-Cladding Interaction	Adds to the random background (diminishes fringe contrast)	Adds to the random background (diminishes fringe contrast)
5.	Temperature Change	Changes scale factor	First order effect
6.	Wavelength Change	Changes scale factor	First order effect

A nine-month program to determine techniques for reducing the noise and obtaining high-sensitivity readout in fiber optic sensors was undertaken. Specific investigations and analyses in support of this objective included: (1) measurement of the effects of mechanical and thermal perturbations on polarization mode coupling in single-mode fibers, (2) measurement of noise in Mach-Zender and Sagnac fiber interferometers, (3) investigation of methods to reduce or eliminate feedback of the transmitted beam into the laser in a Sagnac gyro, (4) analysis of techniques for producing a controllable and

precisely measurable phase bias for the gyro, and (5) assessment of detection, readout, and processing schemes for the gyro. While effort was expended in each of the five areas listed above the bulk of the effort concentrated on Tasks 1-3.

2.0 TECHNICAL DISCUSSION

This effort addressed several unresolved questions related to noise sources and readout techniques for fiber optic sensors. The tasks were divided into two fundamental areas: (1) an experimental investigation of polarization noise in single mode fibers, and (2) a tradeoff study of readout schemes for the fiber optic gyro. Each of these areas of investigation is discussed in some detail below.

2.1 Polarization Noise Experiments

When linearly polarized light is coupled into a typical commercial single-mode fiber, it is found that the polarization of the transmitted light is strongly affected by small perturbations applied along the length of the fiber. The perturbation can be thermal in nature (as produced, for example, by holding a lighted match nearby) or mechanical (produced by forming a loop in the fiber). Some fibers are even sensitive to being touched lightly. When the perturbation is applied with the fiber ends held rigidly in place, the power transmitted through the fiber followed by an analyzer is observed to vary rapidly as a function of time, often going through several maxima and minima.

The sensitivity of single-mode fibers to these perturbations is a consequence of the fact that such fibers actually support two orthogonally polarized modes of propagation. Mechanical and thermal perturbations cause

coupling between these modes, which results in a change in the output polarization.

When linearly polarized light is coupled into a single mode fiber, the output will in general be elliptically polarized. However, there are always two orthogonal orientations for the input polarization which yield a linearly polarized output.[16] If the output polarization is linear for a given orientation of input polarization, then mode coupling resulting from a mechanical or thermal perturbation will cause the output polarization to become elliptical. When such a perturbation is applied, it is necessary to rotate the input polarization to restore a linearly polarized output.

It has been suggested that, in the case of a Sagnac gyro, random fluctuations in fringe positions can be eliminated by the use of analyzers to ensure that only one polarization "channel" can propagate through the fiber to the beam splitter and output photodetector in each direction.[16,17] Although greatly improved fringe stability has been observed by the use of this technique for eliminating nonreciprocal propagation in the Sagnac configuration, the remaining noise is still unacceptably large for practical instruments.[18] For example, the noise observed in Sagnac gyro experiments conducted at the University of Utah Research Institute, with linear polarizers in place, was about three orders of magnitude above the quantum limit. Apparently, temporal and spatial fluctuations in the fiber give rise to significant mode coupling noise even when polarizers are used.

In the fiber optic hydrophone, with the Mach-Zender configuration, polarization coupling effects will also be present. The use of polarizers should lead to considerable noise reduction in this case as well, but polarization mode coupling will still give rise to amplitude fluctuations (fading) as well as relative phase shifts for the two beams. The inherent nonreciprocity of this type of interferometer should in fact result in a much higher polarization noise level than for the Sagnac configuration.

One obvious approach to reduce noise in fiber interferometers is to use a highly birefringent fiber and excite only one polarization mode. The large difference in propagation constants for the two modes should greatly reduce the mode coupling caused by small thermal or mechanical perturbations. A second approach is suggested by the discovery that twisting a conventional round-core fiber can greatly reduce the perturbation-induced polarization shifts. This phenomenon has not yet been explained satisfactorily, although it appears that the twisting may induce a circular birefringence in the fiber.

Two experimental setups have been constructed at Rockwell to investigate polarization noise in single-mode fibers and fiber optic sensors. The first of them, a Sagnac gyro mounted on a rotation table, is illustrated schematically in Fig. 6 and depicted in the photographs of Figs. 7 and 8. With this apparatus, it will be possible to measure the noise in the Sagnac gyro for different fiber types and under different stress conditions. The mount can be filled with index matching fluid to suppress extraneous reflection from the optical surfaces. This should virtually eliminate the noise due

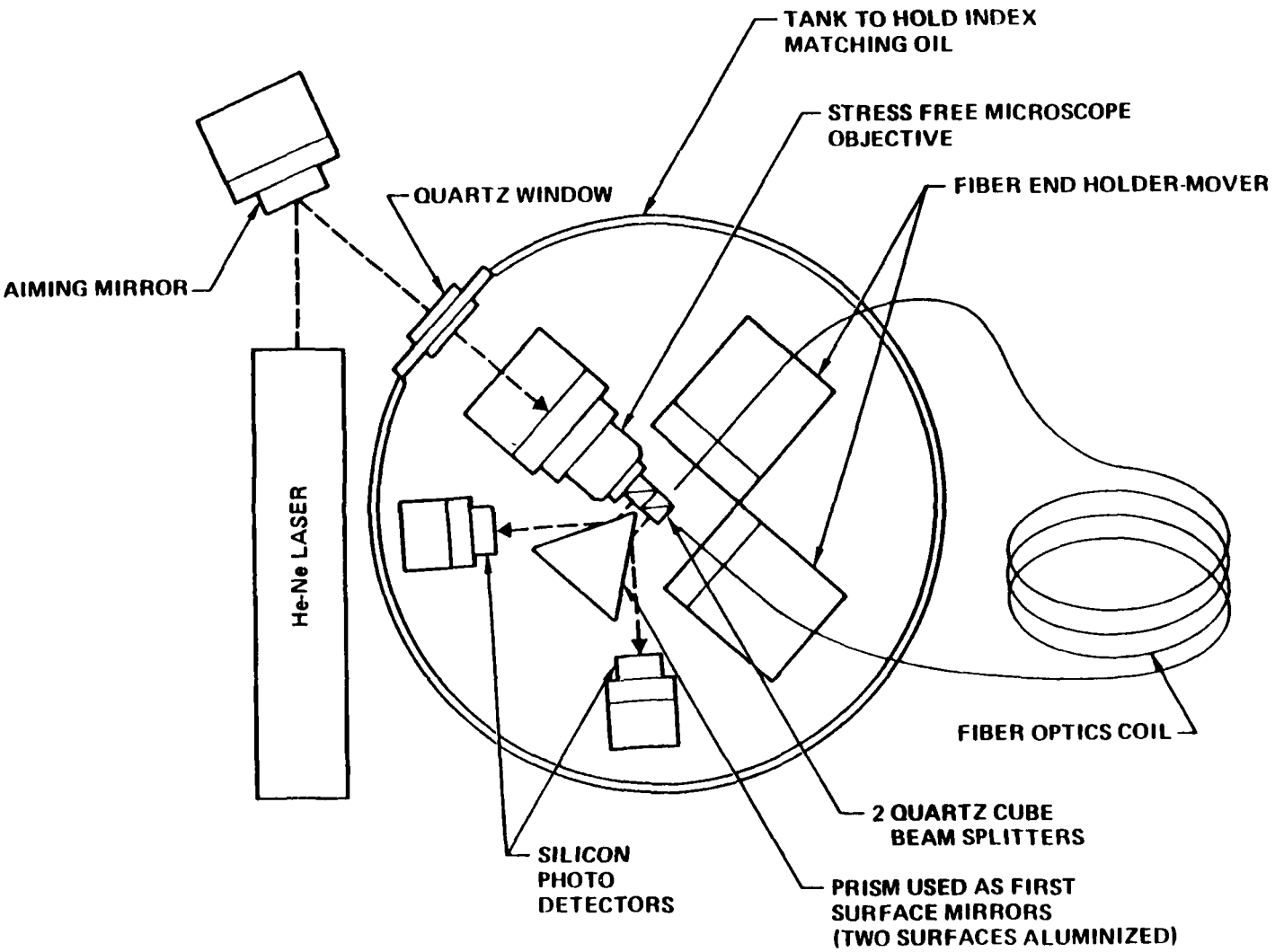

Fig. 6 Configuration of optical components in the fiber ring interferometer.

Fig. 7 Fiber ring interferometer - top view.

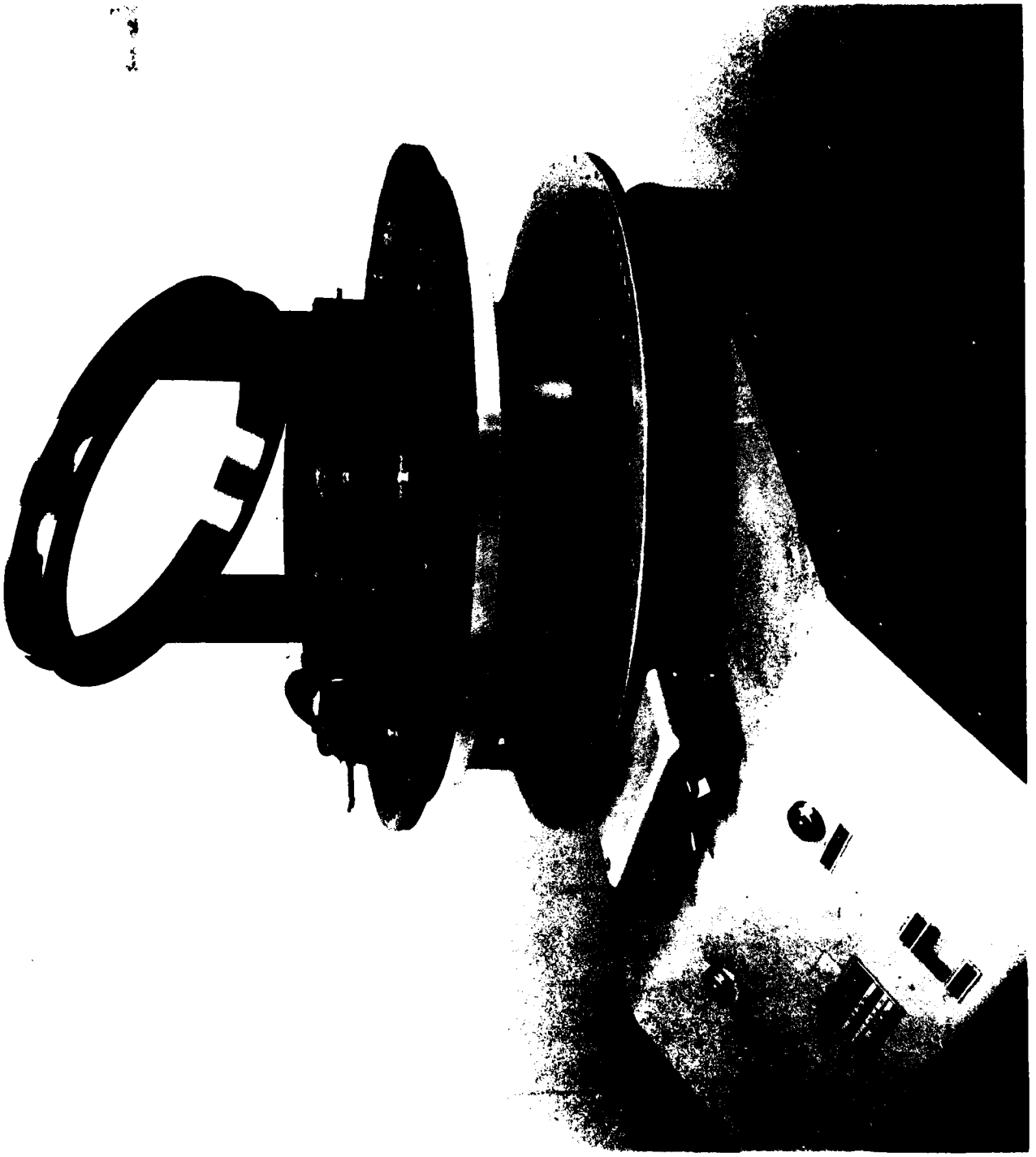

Fig. 8 Side view of fiber rong interferometer mounted on rotation table.

to mechanical motion of components, so that the observed noise is expected to be that generated in the fiber itself.

To study optical hydrophone related noise effects, an extra beam splitter will be added to the experimental setup illustrated in Figs. 6-8 to convert it to a Mach-Zender interferometer.

The second setup for studying polarization noise effects is illustrated schematically in Fig. 9. In this setup, linearly polarized light is coupled into a fiber, with the plane of polarization rotating as a function of time. The output of the fiber propagates through an analyzer, which rotates at 16 times the rate of the input polarization. The transmitted light is detected, and the photodetector output is displayed on an oscilloscope. In such a display, the horizontal (time) axis corresponds to the input polarization angle. Orientations of the input polarization which yield linear output polarization correspond to regions where the oscilloscope trace oscillates between zero and 100% transmission. The output is elliptically polarized where the minima are greater than zero and the maxima less than 100%, and circularly polarized (corresponding to 90° phase shift) where the minima and maxima are equal in amplitude. In general, the phase shift between the linear-to-linear polarization channels, $\Delta\phi$, is given by

$$\Delta\phi = \left\{ 2 \tan^{-1}\left[\frac{P_{min}}{P_{max}}\right]^{1/2} \right\} \begin{array}{l} \text{Maximum over all input} \\ \text{polarization orientations} \end{array} \qquad (2)$$

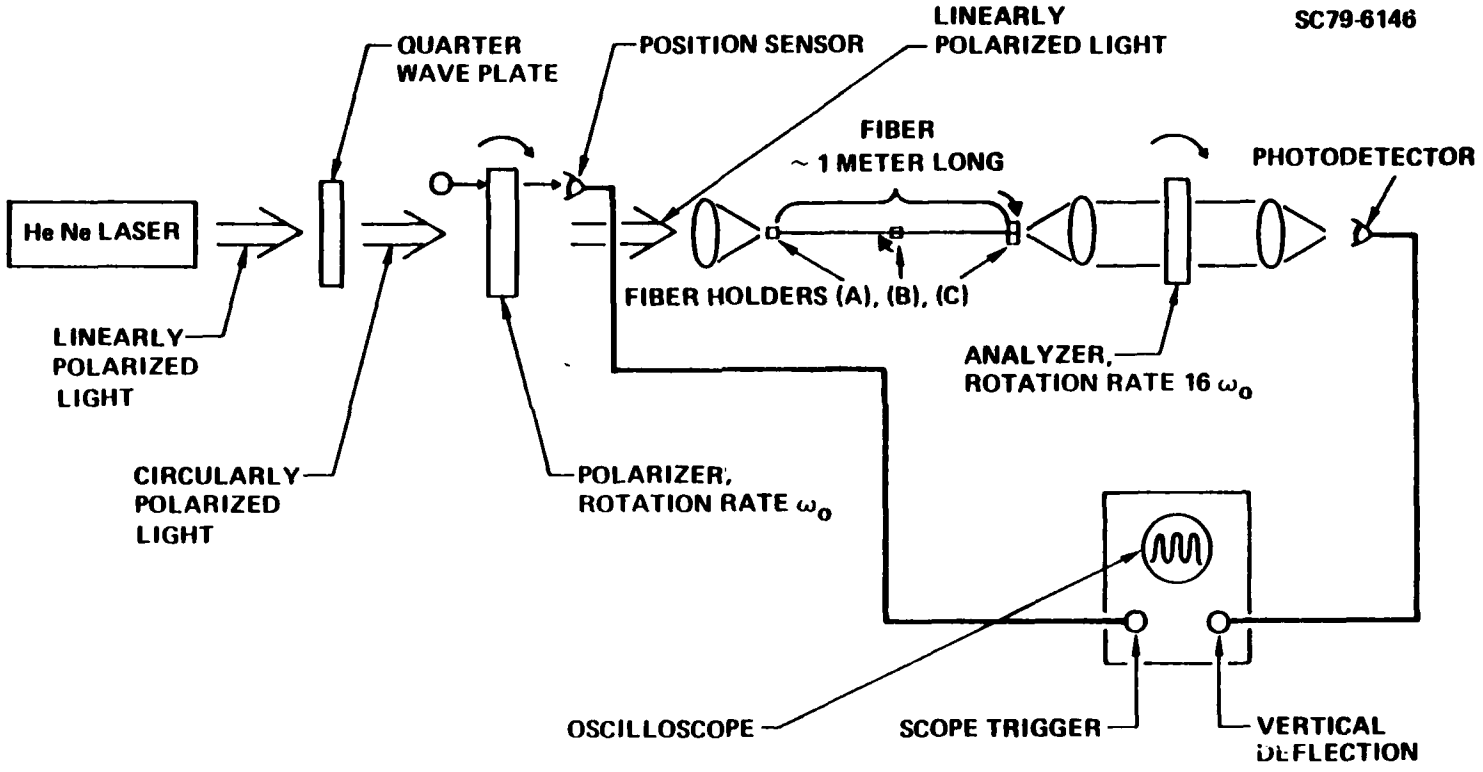

Fig. 9 Experimental setup for investigating fiber polarization mode coupling effects. The photodetector output is displayed on an oscilloscope as a function of angular orientation of input polarization. Note the three fiber holders: (a) fixed, (b) for applying a mechanical perturbation midway along the fiber length, and (c) for twisting the fiber about its axis.

where P_{min} and P_{max} are the (local) minimum and maximum power transmitted through the output analyzer.

The setup illustrated in Fig. 9 is also provided with a means to rotate the output end of the fiber about its axis to produce a measured twist, and to apply a mechanical perturbation at the midpoint of the fiber in the form of a rotation about its axis, with both ends held fixed. Two examples of oscilloscope tracings taken with this setup are shown in Fig. 10. The photographs correspond to two different twist angles (145° and 258°) of the same single-mode fiber. In Fig. 10a, the output polarization changes from linear to elliptical ($\Delta\phi$ = 44°) as the input polarization is rotated. In Fig. 10b, the output polarization is almost circular ($\Delta\phi$ = 83°) for a particular orientation of the input polarization. In order to display the evolution of the output polarization characteristics as a function of twist, a stepped motion picture camera is used to take a sequence of photographs of the oscilloscope, each corresponding to a different twist angle. The resultant "movie" presents a large amount of data in a form that can be readily analyzed.

In order to meet the program objective, experiments using both the apparatus in Figs. 6-8 and the one in Fig. 9 were carried out. The measurements will be made for round core and birefringent polarization-maintaining single mode fibers in unstressed, twisted, and mandrel-wound configurations. The birefringent fibers to be used consisted of a sample previously supplied by Bell Laboratories. The effects of mechanical and thermal perturbations on polarization mode coupling were characterized quantitatively for each of the fiber types and stress conditions indicated above, using the apparatus of

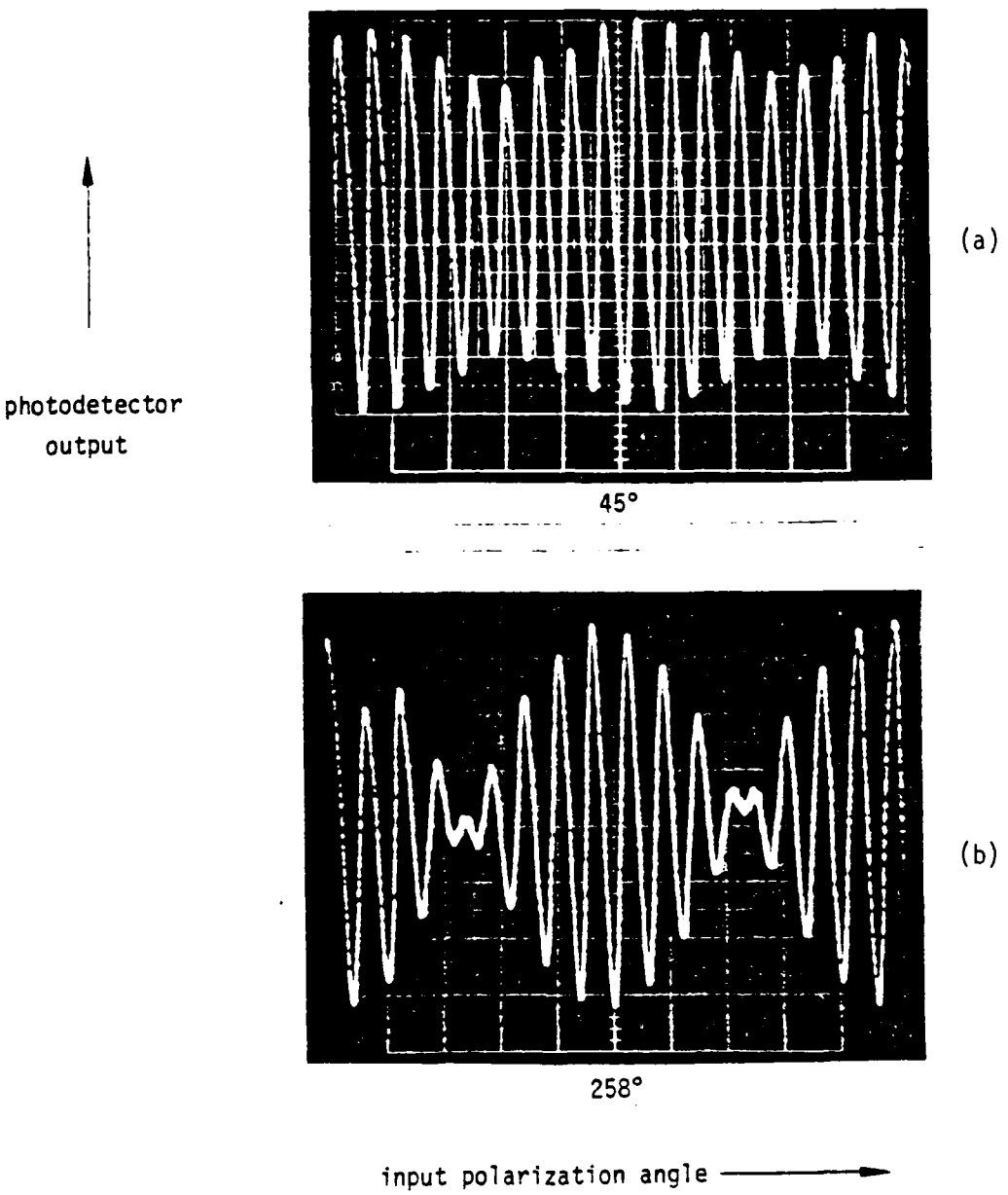

Fig. 10 Examples of oscilloscope tracings obtained with the apparatus of Fig. 4, for twist angles of 45° and 258°. The input polarization angle rotates through 180°, while the output analyzer goes through 8 complete rotations.

Fig. 9. Then, polarization noise was measured for each fiber type and stress condition in the Sagnac interferometer of Fig. 6-8, and in a Mach-Zender interferometer produced by inserting a second beam splitter in the Sagnac apparatus. An effort was made to correlate the results of the two sets of experiments, i.e., to determine if the fibers which are less susceptible to polarization noise due to a mechanical or thermal perturbation also show lower noise in Mach-Zender and Sagnac interferometers.

2.2 Fiber Gyroscope Design

A number of couplex issues must be addressed in the design of a practical fiber optic gyroscope.[19] This analysis addresses some of the most critical of these issues, including techniques for suppressing coupling of the transmitted light into the laser source, methods for producing a controllable phase shift, and readout techniques for achieving high sensitivity. The basic gyro configuration assumed in the analysis is illustrated in Fig. 11.

2.2.1 Suppression of Coupling of Transmitted Light into Laser Diode

Feeding light from an injection laser which is transmitted through the fiber back into the laser cavity can cause mode instabilities leading to unacceptably high noise levels for the gyro application. Alternative means for suppressing this potential noise source which will be compared include the use of a magneto-optic Faraday rotator, pulsing the laser current, and modulating the output of a cw laser in pulsed fashion.

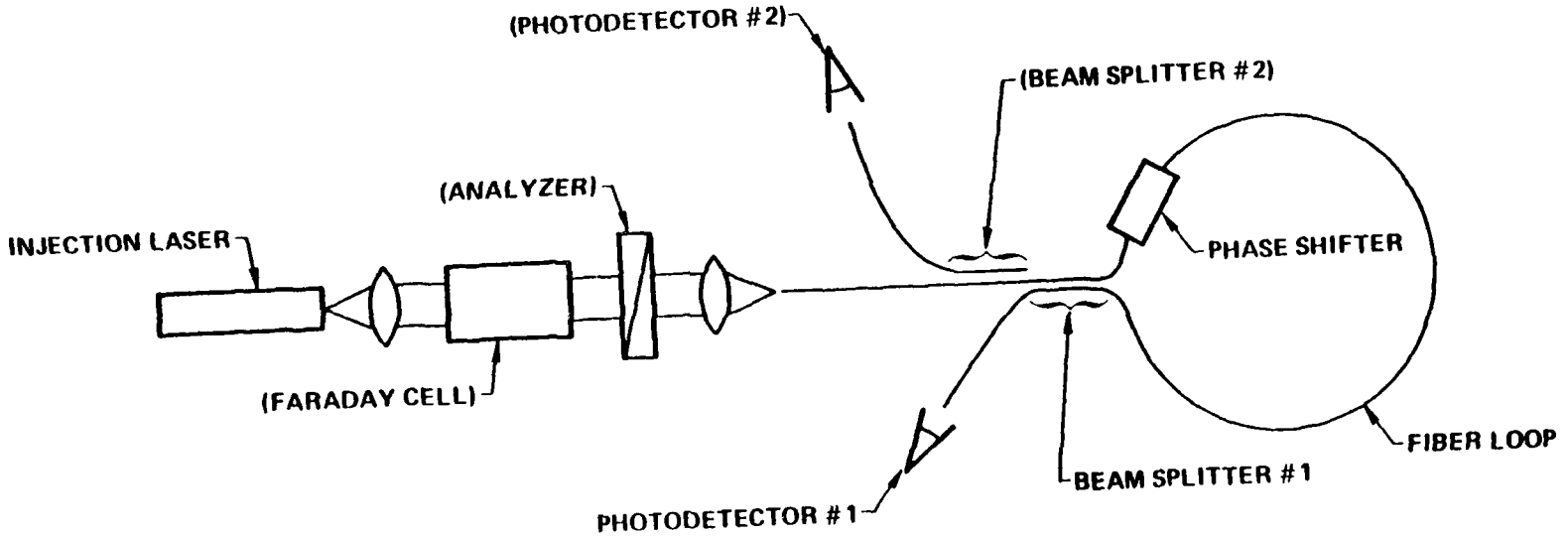

Fig. 11 Configuration for Sagnac gyro assumed for purposes of discussions in the text. Elements with labels in parentheses are not essential for operation of the gyro.

The magneto-optic scheme would make use of a Faraday cell to rotate the laser output polarization by 45° followed by an analyzer oriented to pass the rotated laser polarization. Light passing through the analyzer and Faraday cell in the opposite direction would arrive at the laser with polarization orthogonal to that of the laser. If necessary, a second analyzer could be provided between the laser and Faraday cell to eliminate this orthogonally polarized component. The chief disadvantage of this approach is the additional complexity introduced into the system, increased difficulty of coupling from the laser to the interferometer due to the additional optical elements, and increased optical loss in the system.

Pulsing the laser is attractive from the standpoint of simplicity. The duration of the laser pulse must be shorter than the fiber transit time of 5μs/km, so that none of the transmitted light reaches the laser while it is turned on. Pulse-to-pulse reproducibility of the laser output is a potential problem with this modulation scheme. Some variation in pulse energy can in principle be observed and corrected for by monitoring the laser output power. This should not prove necessary, however, if a two-detector readout scheme with a dynamic phase shift to balance the detector outputs is used. Changes in the spectral content on a pulse-to-pulse basis would be a more serious problem, since wavelength is a part of the scale factor for the gyro.

An external electro-optic modulator can be used in conjunction with a cw laser to produce short pulses which are blocked from feeding back into the laser cavity. However, this wastes laser power, since the laser is emitting even when the modulator is blocking. Additional loss and complexity are also

introduced. However, if it develops that pulse-to-pulse reproducibility in the pulsed laser is a very severe problem, this alternative could prove acceptable.

2.2.2 Methods for Producing a Controllable Phase Shift

The ability to produce a controllable relative phase shift between the counterpropagating beams in the Sagnac gyro is necessary to obtain maximum response in detector output as a function of rotation-induced phase shift and to remove the ambiguity in direction of rotation near rotation rates which induce an integral number of π-radian phase shifts. Perhaps even more significant is the simplicity introduced by a readout scheme which uses such a phase shift in a feedback loop to balance the output of the two complementary photodetectors. Rotation rate is then read out as the amplitude of the induced phase shift.

A Bragg cell can be used to produce a controllable phase shift in the Sagnac gyro.[6] The Bragg cell is inserted between the beam splitter and one of the fiber ends, and the first-order acoustically diffracted beam is focussed onto the fiber end. The phase shift for the counterpropagating beams is determined as the change in phase in the acoustic wave which occurs during the optical transit time for the fiber.[19] An attractive readout scheme is to vary the acoustic frequency in a feedback loop to balance the dc signals from two complementary photodetectors. The advantage is that the phase shift can be read out in digital fashion by counting zero crossings for the oscillator which drives the Bragg cell. The disadvantage lies in the additional

complexity and optical loss resulting from inserting the Bragg cell in the fiber loop, and a large additional noise component could also result from ambient mechnical or normal perturbation acting on the Bragg cell. A very stable oscillator is also required for high sensitivity, and the frequency dependence of Bragg-cell-to-fiber coupling efficiency is also a matter of concern.

An electro-optic or magneto-optic phase shifter can also be used with reciprocal propagation channels if the laser source is pulsed. The phase shifter is located between the beam splitter and one fiber end, as in the case of the Bragg cell. The bias voltage or current applied to the phase shifter is changed during the optical transit time for the pulse, so that the relative phase shift is proportional to the change in bias. The electro-optic phase shifter would operate on linearly polarized light, while use of the magneto-optic shifter would require that the counterpropagating beams be circularly polarized. The phase shifter would introduce additional complexity and optical loss in the interferometer optical path. Furthermore, readout of the phase shift would require the measurement of an analog quantity (the voltage or current change for the phase shifter) and would be less precise than the counting technique applicable to the acousto-optic modulator.

Other methods for producing the phase shift would make use of either linear or circular birefringence of the fiber or another optical element inserted in the interferometer. In each of these schemes, the counter propagating beams excite eigen modes with different propagation constants, β_1 and β_2, and the relative phase difference is $(\beta_1-\beta_2)$ L, where L is the path

length. If linear birefringence of the fiber is used, then linearly polarized light is coupled into the fiber ends, and a dc-biased electro-optical phase shifter can be used to control the relative phase difference. If circular birefringence is used, then the fiber inputs must be circularly polarized, and the Faraday effect or twist-induced optical activity can be used to control the relative phase difference. All of these schemes would have the disadvantage of potentially higher noise and phase drift due to noncommon propagation "channels" in the fiber. It would also be necessary to read an analog voltage or current to determine the phase shift.

2.2.3 Readout Schemes and Other Design Considerations

A practical design for a fiber optic gyro must not only provide for high sensitivity (10^{-6}-10^{-7} fringe for an inertial grade instrument), but it should be inherently simple, low in cost, and reliable. The preceding discussions of the specific problems of polarization noise, feedback of transmitted light into the laser, and of ways to produce a controllable phase shift, have already alluded to a number of tradeoffs which must be considered in gyro design. Other tradeoffs have to do with the detection scheme (homodyne or heterodyne) and the way in which the photodetector outputs are processed (single detector, difference between two detector outputs, ratio of detector outputs or balanced detector with feedback to the phase shifter). It can be assumed that the gyro output will be digital or will eventually be converted to digital form, but the role of digital processing in determing the rotation rate from the raw data must be decided. For example, with an acousto-optic

phase shifter with feedback from balanced detectors, the Bragg cell frequency and therefore the phase shift are readily determined in digital form by counting zero crossings. If balanced detection is not used, on the other hand, the photodetector outputs might be digitized and directly fed into a microprocessor, along with a digitized value for the induced phase shift, and the rotation rate computed by the microprocessor. Techniques for correcting for temperature variations, variation in laser power or wavelength, and other factors must also be determined.

Some of the most important tradeoff factors are summarized in Table II. These were investigated during the course of this effort.

Table II

Gyro Design Tradeoffs
(Sheet 1 of 2)

Design Factor	Advantage	Disadvantages/Problems
	LASER MODULATION	
Pulsed	Suppresses feed back to laser	Pulse-to-pulse reproducibility a problem
	Facilitates sampling/digital processing	
Sinusoidal	Allows phase-sensitive detection	Requires Faraday cell to avoid feedback to laser Frequency shifts in laser a potential problem
cw	Laser characteristics stable	Requires Faraday cell
	COUPLING FROM LASER TO FIBER BEAM SPLITTER	
Direct (e.g., with microlens)	Simple	Pulsed laser needed to eliminate feedback
Through Faraday cell	Relatively complex Extra optical loss	Can use cw or sinusoidally modulated laser
	PHASE SHIFTER (RECIPROCAL CHANNELS)	
Bragg cell	Allows digital readout	Requires stable oscillator Optical transmission a function of phase shift
Electro-optic or Magneto-optic (Pulsed)	More easily implemented than Bragg cell	Analog readout of phase Requires pulse-to-pulse reproducibility and low drift during pulse

Table II

Gyro Design Tradeoffs
(Sheet 2 of 2)

Design Factor	Advantage	Disadvantages/Problems
	PHASE-SHIFTER (NON-RECIPROCAL CHANNELS)	
Electro-optic Crystal or Faraday cell	More easily implemented than Bragg cell	Requires optical device in interferometer Non-reciprocal channels can cause noise and drift
Twist-induced birefringence	No additional optical element in interferometer	Same as above, not rapidly variable
	DETECTION SCHEMES	
Homodyne	Simple	Less sensitive; susceptible to low frequency noise
Heterodyne	Higher sensitivity Avoids low frequency noise	Relatively complex Non-common paths introduce possible thermal drift
	DETECTOR PROCESSING	
Single detector, or two-detector differential	Simple	No compensation for laser variations
Two-detectors, ratio	Compensates for laser power variation	More complex signal processing electronics
Balanced detectors, with feedback to phase shifter	Compensates for laser power variation Maintains maximum rotation rate sensitivity Does not require processing of detector output	Complexity of feedback loop

3.0 EXPERIMENTAL RESULT

3.1 Coupled Mode Theory for Twisted Fibers

Propagation of light in a twisted single mode fiber can be analyzed in a simple and straightforward manner using coupled mode theory. The fiber is assumed to be a birefringent medium with principal axes which rotate about the fiber axis as the end of the fiber is twisted. The coupled mode analysis considers the variation in amplitude of the two local round modes of the fiber as a function of distance along the fiber axis. The "weakly guiding" approximation is assumed, so that the polarization of the normal modes is approximately linear. Polarization vectors for these modes are directed along the axes of birefringence of the fiber, which are also the axis of the local coordinate system. The axes of the local coordinate system then rotate as the end of the fiber is twisted.

To characterize the fiber twist in terms of the coupled mode theory, it is useful to first consider the propagation of an incident wave through a birefringent plate of length δz. The light is assumed to propagate in the z-direction. The first plate is in contact with a second plate identical to the first, but with birefringence axes rotated through an angle $\delta\theta$ about the z-axis with respect to the first plate. Assuming that the incident wave amplitudes are a and b, corresponding to field components polarized along the respective axes of the first plate, the amplitude after transmission through that plate, a" and b", are given by

$$\begin{bmatrix} b'' \\ a'' \end{bmatrix} = \begin{bmatrix} e^{i\beta_a \delta z} & 0 \\ 0 & e^{i\beta_b \delta z} \end{bmatrix} \begin{bmatrix} a \\ b \end{bmatrix} \tag{3}$$

where β_a and β_b are the propagation constants corresponding to the respective axes of propagation.

Upon entering the second plate, the local normal mode amplitudes transform according to

$$\begin{bmatrix} a' \\ b' \end{bmatrix} = \begin{bmatrix} \cos(\delta\theta) & -\sin(\delta\theta) \\ \sin(\delta\theta) & \cos(\delta\theta) \end{bmatrix} \begin{bmatrix} a'' \\ b'' \end{bmatrix} \tag{4}$$

Combining these two matrix expressions, and retaining only the terms to first order in $(\delta\theta)$ (δz), yields

$$\begin{bmatrix} a' \\ b' \end{bmatrix} = \begin{bmatrix} e^{i\beta_a \delta z} & -\delta\theta \\ \delta\theta & e^{i\beta_b \delta z} \end{bmatrix} \begin{bmatrix} a \\ b \end{bmatrix} \tag{5}$$

Thus, in the limit of small $\delta\theta$ and δz, this reduces to

$$a' = ae^{i\beta_a \delta z} - \delta\theta b$$

$$b' = \delta\theta a + be^{i\beta_b z} \tag{6}$$

If we let $A = ae^{i\beta_a z}$, $B = be^{i\beta_b z}$, then the difference equations above can be expressed in the differential forms

$$\frac{dA}{dz} = \kappa B e^{-\Delta z}$$

$$\frac{dB}{dz} = -\kappa A e^{i\Delta z} \tag{7}$$

where $\kappa = -\frac{d\theta}{dz}$ and $\Delta = \beta_b - \beta_a$. Equations (1) and (2) are the coupled mode equations, which are readily solved in close form if κ_{ab} and Δ are uniform in the z direction. The result is

$$\begin{bmatrix} A(z) \\ B(z) \end{bmatrix} = \begin{bmatrix} M_2 e^{-i\Delta z/2} & M_1 e^{-i\Delta z/2} \\ -M_1 e^{i\Delta z/2} & M_2 e^{i\Delta z/2} \end{bmatrix} \begin{bmatrix} A(0) \\ B(0) \end{bmatrix} \tag{8}$$

where $M_1 = \frac{\kappa}{\alpha} \sin(\alpha z)$, $M_2 \cos(\alpha z) + \frac{i\Delta}{2\alpha} \sin(\alpha z)$ and $\alpha = \sqrt{\kappa^2 + (\frac{\Delta}{2})^2}$.
Setting $A(o) = a$, $B(o) = b$, $A(z) = A(z) = a'e^{i\beta_a z}$, $B(z) = b'e^{i\beta_b z}$ yields the even simpler expression

$$\begin{bmatrix} a' \\ b' \end{bmatrix} = \begin{bmatrix} M_2 & M_1 \\ M_1 & M_2^* \end{bmatrix} \begin{bmatrix} a \\ b \end{bmatrix} e^{-i(\beta_a + \beta_b)z/2} \tag{9}$$

relating the amplitudes of the local normal modes after propagating a distance z to the incident mode amplitudes.

The matrix equation above completely describes propagation in a twisted single-mode fiber. However, the value of κ given above must be modified to take into account the twist-induced circular birefringence term first observed and analyzed by Ulrich.[20] The modified expression is $\kappa = -\frac{d\theta}{dz}(1 - g/2)$, where $g = 0.16$ for silica fibers. It has also been tacitly assumed that the spatial variations in electric field amplitude are identical for the two orthogonally polarized local normal modes. This will not be true in the general case, but for weakly guiding fibers the correction for this effect can be considered negligible.

In general, if linearly polarized light is coupled into a single-mode fiber, the transmitted light will be linearly polarized, elliptically polarized, or circularly polarized. However, there are always two orthogonal orientations of the input polarization which yield a linearly polarized output. For the uniformly twisted birefringent single mode fiber, it is

possible to determine the required rotation of input polarization in terms of the matrix element M_1 and M_2. To do this, we define new coordinate systems in input and output planes, rotated by angle θ_1 and θ_2 with respect to the original coordinate systems with axes parallel to the birefringence axes of the fibers. The amplitudes of the two polarization components of the input beam, a_1 and b_2, are related to the amplitudes in the output coordinate system, a_2 and b_2, by

$$\begin{bmatrix} a_2 \\ b_2 \end{bmatrix} = \begin{bmatrix} \alpha_2 & \beta_2 \\ \beta_2 & \alpha_2 \end{bmatrix} \begin{bmatrix} M_2 & M_1 \\ -M_1^* & M_2^* \end{bmatrix} \begin{bmatrix} \alpha_1 & -\beta_1 \\ \beta_1 & \alpha_1 \end{bmatrix} \begin{bmatrix} a_1 \\ b_1 \end{bmatrix} \tag{10}$$

where $\alpha_i = \cos \theta_i$, $\beta_i = \sin \theta_i$, $i = 1,2$. The amplitude a_1, b_1, a_2, b_2, are measured in the new, rotated coordinate system. After performing the matrix multiplication, the preceding equation reduces to

$$\begin{bmatrix} a_2 \\ a_1 \end{bmatrix} = \begin{bmatrix} u & w \\ -w^* & v \end{bmatrix} \begin{bmatrix} a_1 \\ b_1 \end{bmatrix} \tag{11}$$

where

$$u = \alpha_2\alpha_1 M_2 - \alpha_2\beta_1 M_1 + \beta_2\alpha_1 M_1^* + \beta_2\beta_1 M_2^*$$

$$v = \beta_2\beta_1 M_2 + \beta_2\alpha_1 M_1 - \alpha_2\beta_1 M_1^* + \alpha_2\alpha_1 M_2^*$$

$$w = \alpha_2\beta_1 M_2 + \alpha_2\alpha_1 M_1 + \beta_2\beta_1 M_1^* - \beta\ \beta_1 M_2^* \quad . \tag{12}$$

A linearly polarized output is obtained if either a_1 or b_1 equals zero, and w = 0. The latter condition can be expressed as

$$\alpha_2\beta_2 M_{2r} + \alpha_2\alpha_1 M_{1r} + \beta_2\beta_1 M_{1r} + \beta_2\alpha_1 M_{2r} = 0$$

$$\alpha_2\beta_1 m_{2i} - \alpha_2\alpha_1 M_{1i} - \beta_2\beta_1 M_{1i} + \beta_2\alpha_1 M_{2i} = 0 \tag{13}$$

After some use of trigonometric identities, we find that, if w - 0, then

$$\tan(\theta_2 - \theta_1) = \frac{M_{1r}}{M_{2r}}$$

$$\tan(\theta_1 + \theta_2) = \frac{M_{2i}}{M_{2i}} \tag{14}$$

Using our previous expressions for M_1 and M_2, it follows from these two equations that $\tan(\theta_1 + \theta_2) = 0$, or $\theta_1 = -\theta_2$,

and

$$\tan(\theta_2 - \theta_1) = \frac{\kappa}{\alpha} \tan(\alpha z) \quad . \tag{15}$$

With $w = 0$, the matrix expression above is diagonal, and the phase difference between u and v determines the maximum ellipticity of the output as the input polarization vector is rotated. Specifically, if $u = ve^{\pm i\psi}$, then if $\psi = N\pi$, $N = 0, 1, 2, 3, \ldots$, the output polarixation will be linear for any orientation of input polarization. On the other hand, if $\psi = (\pm N + \frac{1}{2})\pi$, $N = 0, 1, 2, 3, \ldots$, the output polarization will be circular if the input polarization is oriented at 45° to the principal axes a_1 and b_1. For other values of ψ, the output will be elliptically polarized unless the input is polarized along the a_1 or b_1 axes.

In order to determine the phase shift ψ, it is first noted that $U = v^*$, so that, when $W = 0$, we can write $U = e^{i\psi/2}$, $V = e^{-1\psi/2}$. But, from the definition of U,

$$U_r = \alpha_2\alpha_1 M_{2r} - \alpha_2\beta_1 M_{2r} + \beta_2\alpha_1 M_{1r} + \beta_2\beta_1 M_{2r}$$

$$U_i = \alpha_2\alpha_1 M_{2i} - \alpha_2\beta_1 M_{1i} - \beta_2\alpha_1 M_{1i} - \beta_2\beta_1 M_{2i} \tag{16}$$

which reduces to

$$U_r = \cos(\theta_1 - \theta_2)\, M_{2r} - \sin(\theta_1 - \theta_2) M_{1r}$$

$$U_i = \cos(\theta_1 + \theta_2)\, M_{2i} - \sin(\theta_1 + \theta_2) M_{1i} \tag{17}$$

But $\tan(\frac{\psi}{2}) = U_i / U_r$, and since $M_{1i} = 0$ and, for $C = 0$, $\theta_1 + \theta_2 = 0$, it follows that

$$\tan\left(\frac{\psi}{2}\right) = \frac{M_{2i}}{\cos(\theta_1 - \theta_2) M_{2r} - \sin(\theta_1 - \theta_2) M_{2r}} \tag{18}$$

Substituting expressions for the matrix elements M_{1r}, M_{2r}, and M_{2i} yields the result

$$\tan\left(\frac{\psi}{2}\right) = \frac{\frac{\Delta}{2\alpha} \sin(\alpha z)}{\cos(\theta_1 - \theta_2)\cos(\alpha z) - \sin(\theta_1 - \theta_2) \frac{\kappa}{\alpha} \sin(\alpha z)} \tag{19}$$

It follows that

$$\sin(\theta_1 - \theta_2) = -\frac{\kappa\frac{\Delta}{2}\sin(\alpha z)}{\sqrt{\kappa^2 \sin^2(\alpha z) + \alpha^2 \cos^2(\alpha x)}} \tag{20}$$

$$\cos(\theta_1 - \theta_2) = \frac{\alpha\cos(\alpha z)}{\sqrt{\kappa^2\sin^2(\alpha z) + \alpha^2\cos^2(\alpha z)}} \tag{21}$$

so that (19) finally simplifies to

$$\tan\left(\frac{\psi}{2}\right) = \frac{\frac{\Delta}{2}\sin(\alpha z)}{\sqrt{\alpha^2\cos^2(\alpha z) + \kappa^2\sin^2(\alpha z)}} \tag{22}$$

The fiber output will be circularly polarized if $\psi = (N + \frac{1}{2})\pi$, $N = 0, \pm1, \pm2, \ldots$; which implies that $\tan(\frac{\psi}{2}) = \pm1$. Thus, circular polarization will occur if

$$\left(\frac{\Delta}{2}\right)^2 \sin^2(\alpha z) = \alpha^2\cos^2(\alpha z) + \kappa^2\sin^2(\alpha z) \quad , \tag{23}$$

or

$$\tan^2(\alpha z) = \frac{\alpha^2}{\left(\frac{\Delta}{2}\right)^2 - \kappa^2} = \frac{\left(\frac{\Delta}{2}\right)^2 + \kappa^2}{\left(\frac{\Delta}{2}\right)^2 - \kappa^2} \tag{24}$$

It follows immediately from this result that the output cannot be circularly polarized in the limit of large τ, or more precisely, if $|\kappa| > |\frac{\Delta}{2}|$.

3.2 Fiber Twist Results

Two different fibers were used in this study: (1) ITT circular core fiber and (2) Bell labs fiber with strain-induced birefringence. Figure 12 shows the dependence of the output polarization angle as a function of the fiber twist for ITT circular core fiber. The fiber was 112 cm long and was truly single mode at λ = 6328 Å. A fiber was held straight with about 50 gm force. An oscilloscope picture similar to Fig. 20 was taken for every 5° increment change of fiber twist. The twisting was started at about five turns in counterclockwise direction (with respect to light propagation direction) and changed through zero twist to about 17 turns in clockwise direction. There are two distinct slopes of this curve. For the first seven turns, the polarization twist slope was about 1. For the remaining 15 turns when the fiber was twisted in the opposite direction, the slope is 1.56. It is seen from the graph (Fig. 12) that the zero twist position was probably at about 7 turns from the starting position. It is also apparent (Fig. 12) that the slope of the output polarization angle versus twist angle has large random fluctuations. When such a fiber is used in a gyroscope, environmental variations produce unacceptably large-amplitude noise.

The Bell Labs fiber used in this experiment has the beat length of 3.3 cm, making the index difference between the fast and slow axes

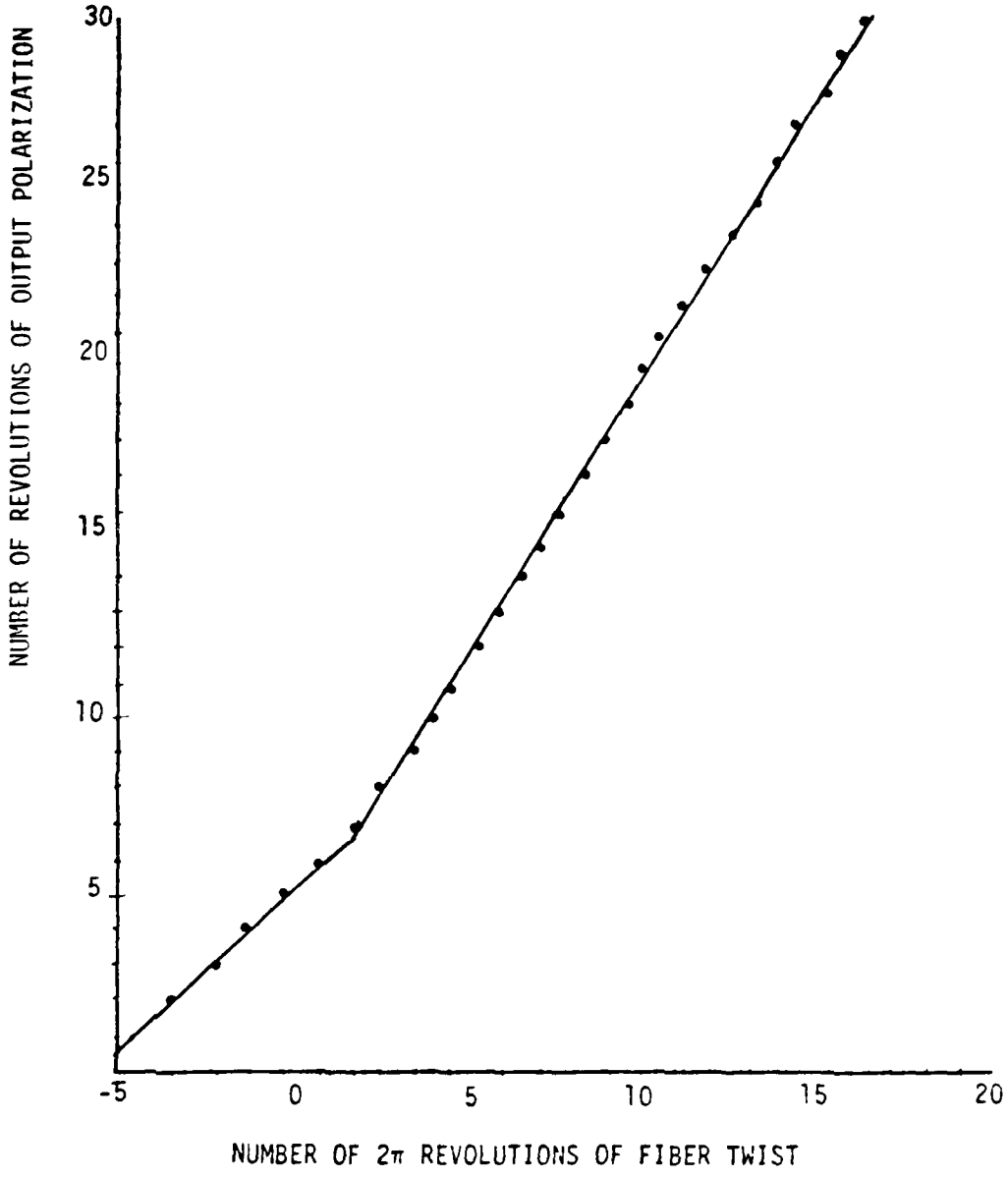

Fig. 12 ITT fiber 112 cm 50 gm tension starting at -5 turns 5° increments.

$30\,\Delta n = 2 \times 10^{-5}$. This is sufficient if one is somewhat careful not to bend the fiber too sharply (bend radius < 1 in.), or heat it too nonuniformly.[5] This fiber has not changed its polarization maintaining properties measurably over a period of one year, indicating that stress relaxation times in these fibers are quite long.

When this fiber is twisted, the plane of polarization follows the twist within the measurement accuracy. (Fig. 13). In this experiment one meter of fiber was used. Over a twist range of -4 to +10 turns, all the small-scale variations in the polarization turning rate were within the readout error. Overall polarization turning rate with respect to the mechanical fiber end turning was within 1% (the readout error). If the polarization maintaining fiber is used in the Sagnac ring interferometer gyroscope, the fiber will be reciprocal only if the direction of polarization coincides with the slow or the fast axes. Otherwise the oppositely traveling beams do not see identical indexes of refraction in the same fiber cross section. (In previous experiments the observed average index difference between oppositely traveling beams was $\sim 5 \times 10^{-12}$.)

The theoretical result indicated in Eq. (24) is compared with experimental data on the Bell Labs polarization maintaining fiber in Table III. The data was obtained by a frame-by-frame analysis of the oscilloscope tracing "movies" obtained by changing the twist angle in 5° increments, from about -4 turns to +9 turns. The twist angles which gave a circularly polarized output were determined as accurately as possible and correspond to the data in the first column of that table. Next, a correlation of 0.19 turns

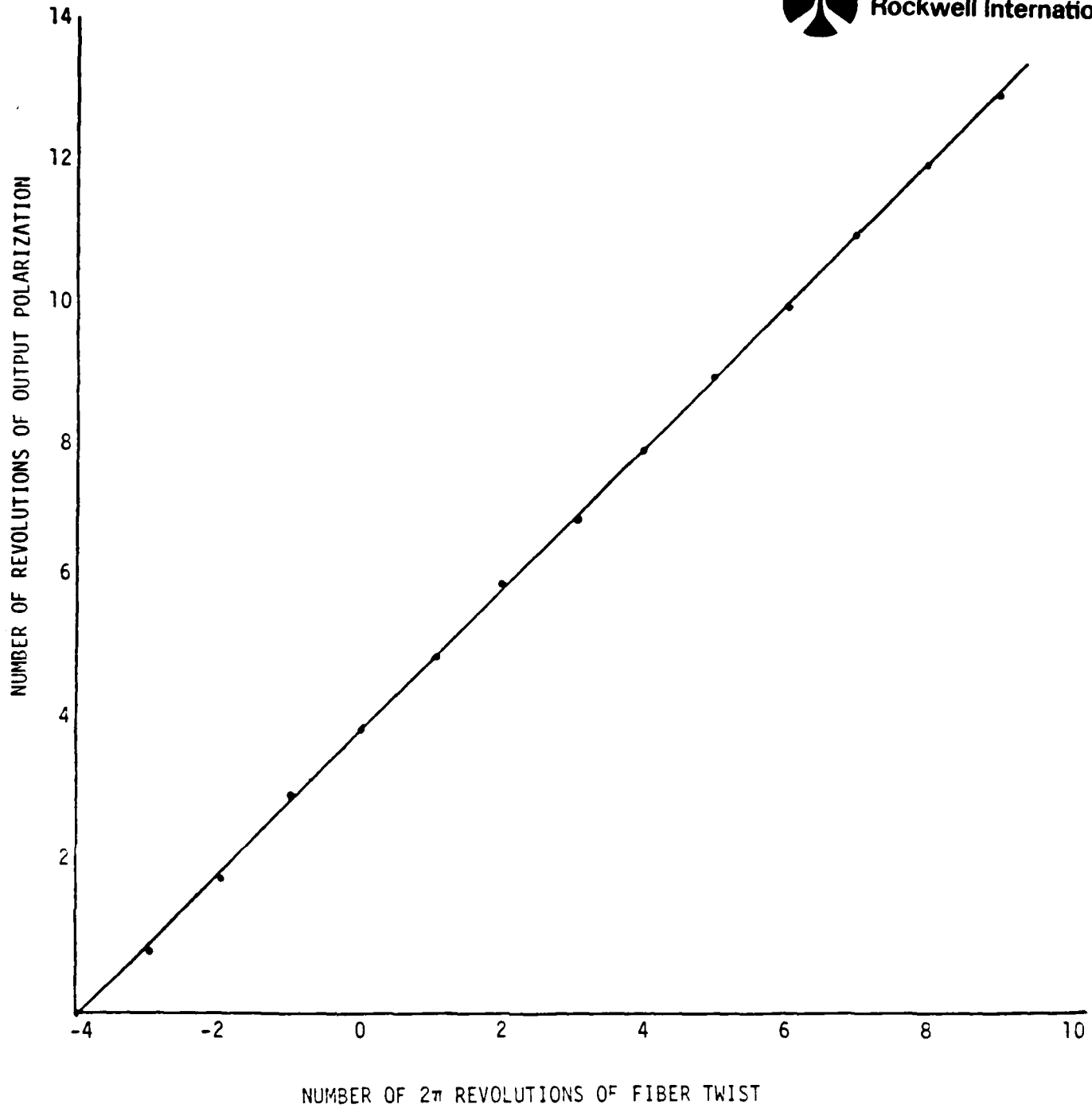

Fig. 13 Bell Labs fiber 104 cm no tension starting at -4 turns 5° increments.

was added to each of those figures to make the twist angles corresponding to the most widely separated zero crossings symmetric about $\tau = 0$. This compensates for an apparent residual twist in the fiber. The values of κ correspond to 0.92 τ, or $0.92 \times 2\pi = 5.78$ radians per turn. The final column is the value of τ for a circularly polarized output calculated from (24), using the value of $L = 210$ radians. This value of L was chosen because it gives a good fit to the data. The difference in effective refractive indices $n_a - n_b = (\Delta L)/2\pi L$ is calculated to be 2.1×10^{-5}, corresponding to a beat length ℓ_b of $\lambda/(n_a - n_b)$ of 3.3 cm for this fiber.

An effort was also made to analyze similar data for conventional, circular core fibers from ITT on the basis of the coupled mode theory. However, it was not possible to obtain a good fit to the data using the simple model.

Table III

Comparison Experimental Data with Calculated Values for Fiber Twist Angle Which Gives a Circularly Polarized Output for Some Orientation of a Linearly Polarized Input

τ Experimental (Turns) Uncorrected	With Zero Corrected	κ(rad)	κ^2(rad^2)	τ Calculated (Turns)
-3.94	-3.75	-21.7	470	-3.81
2.17	-2.08	12.0	145	-2.20
1.89	2.08	12.0	145	2.20
3.50	3.69	21.3	455	3.81
4.73	4.92	28.4	809	4.83
5.64	5.83	33.7	1136	5.76
6.50	6.69	38.7	1496	6.35
7.24	7.43	43.0	1845	7.18
7.99	8.18	47.3	2236	7.67
8.56	8.75	50.6	2558	8.34

The coupled mode theory can therefore be used with considerable confidence to explain the polarization behavior in polarization maintaining Bell fiber. However, because of the random distribution of stresses (produced during manufacturing process and by random bending, twisting and temperature variations) the polarization of ITT fiber is still intractable.

3.3 Fiber Heating Results

In another experiment the state of polarization at the output of the Bell labs fiber was determined when thermal perturbation is applied.[5] The temperature of the fiber was temporally and spatially randomly varies ~ 20°C over 60 cm length. The polarization was swept through an angle of about 90° for Fig. 14a (30 times) and about 180° for Fig. 14b (5 times). It is seen that at temperatures where the index difference between the fast and slow axis is such that the fiber behaves almost like a quarter wave plate, the exit phase varies quite drastically with the perturbation. However, when the direction of polarization of the light entering the fiber coincides with the fast or slow axes, the phase is unchanged by the external perturbation. These directions are marked in Fig. 14 with F.

3.4 Sagnac Interferometer Noise Study

Rotation sensing fiber Sagnac ring interferometers have the potential of becoming rugged, passive, virtually no maintenance alternatives to mechanical or ring laser gyroscopes. The projected shot noise limited accuracy is sufficient for navigation (drift $< 10^{-3}$ deg/hr).

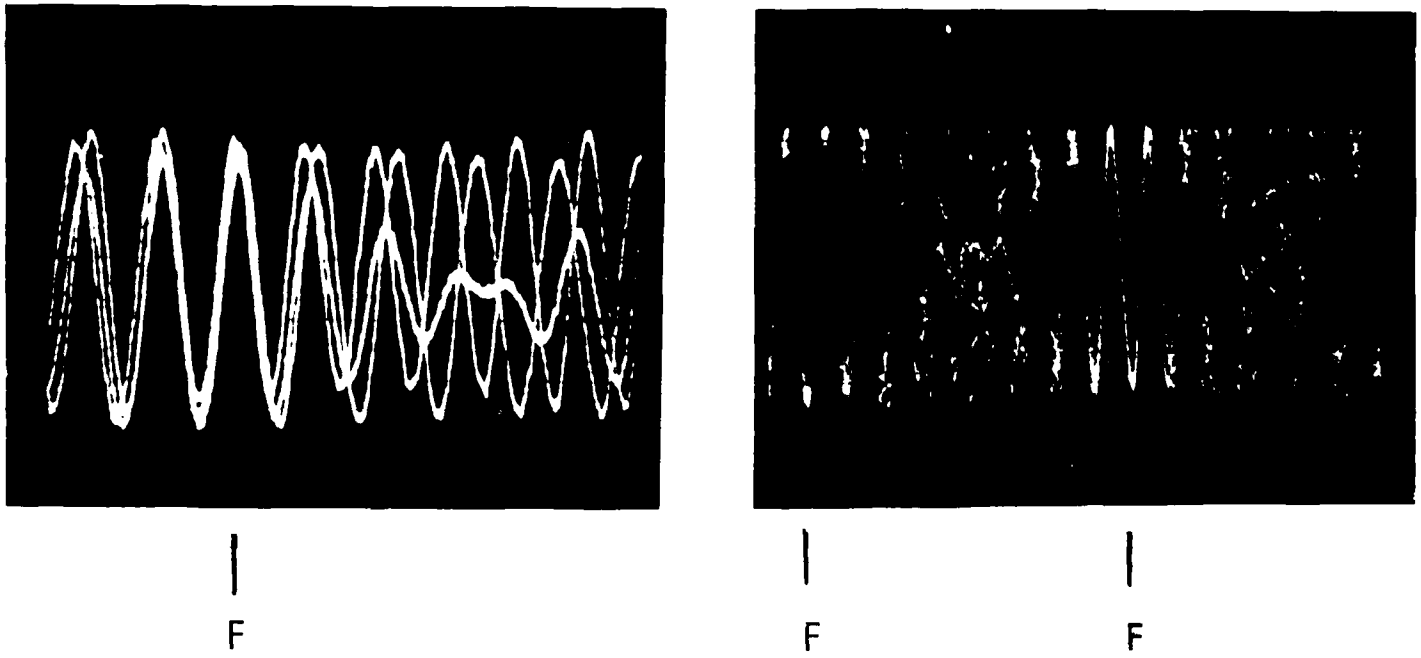

Fig. 14 The behavior of polarization in Bell Lab's fiber when it is heated nonuniformly about 20°C. At slow and fast axis of the fiber the phase of polarization remains constant. (Points F).

There are three major noise sources that limit the accuracy:

1. Unwanted reflections in the optical path of the interferometer that produce additional fringe patterns superimposed on the Sagnac fringes.

2. Polarization noise, and

3. Interferometer component motion that produces nonreciprocity in the external (to the fiber) beam path. This includes also small variations in the beam direction.

In a circular core fiber the state of polarization is scambled over a short distance in the fiber. This means that the oppositely traveling beams do not see the same index of refraction at an arbitrary point in the fiber, producing nonreciprocity variations as the acoustic noise and the temperature varies.

The fiber Sagnac interferometer used in the present experiment eliminates two of these difficulties. Figure 15 shows the experimental configuration of the interferometer components. A cw current stabilized diode laser was used as the light source (λ = 8500 A). A microscope objective produces a parallel beam. To obtain linearly polarized light a Glan-Thompson prism is placed in the beam path. Two cube beamsplitters are used such that both complementary Sagnac fringe patterns can be observed. A short, 6.2 meter

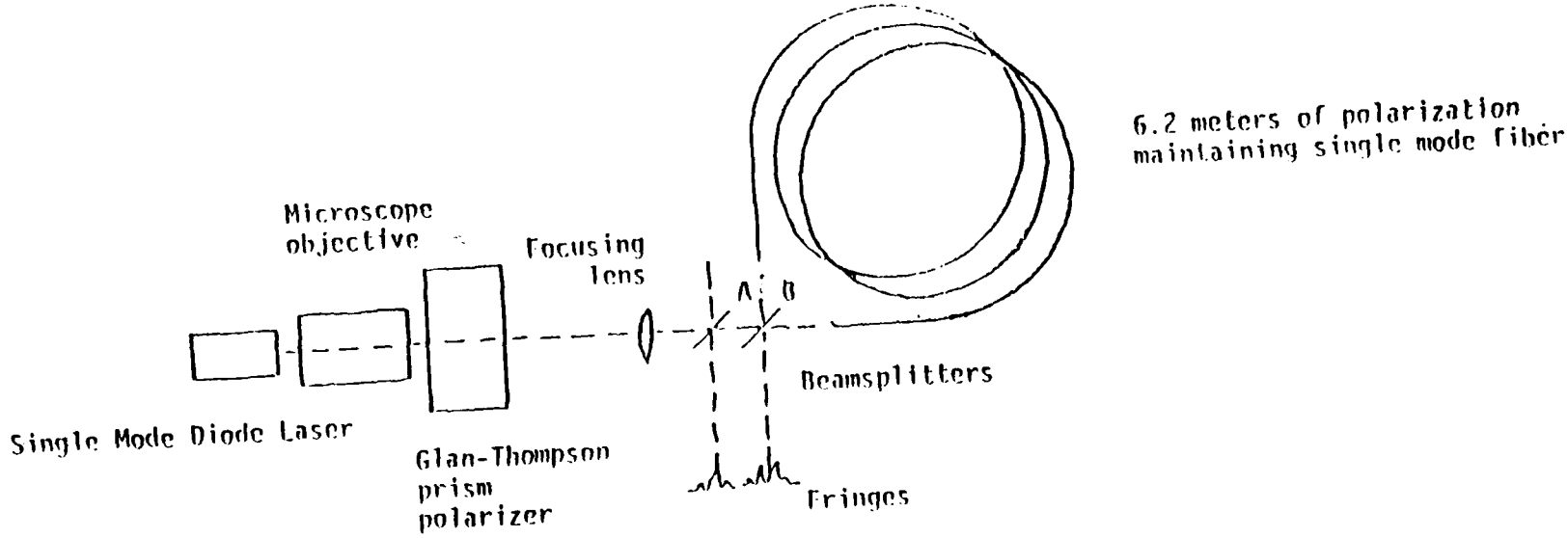

Fig. 15 Schematic diagram of fiber gyro with polarization maintaining fiber.

polarization maintaining fiber forms the Sagnac gyro beam path. It was made by ITT and has beat length equal to 0.9 cm. Stress produced birefringence maintains the polarization. Some care in handling the fiber is necessary because of the relatively long beam length. Either the fast or the slow axes can be used for the beam path. The method of finding the axes used in this experiment was to slowly change the input polarization angle and minimize the output polarization change as the fiber is repeatedly heated and cooled. This allows one to find the fast or slow axes with accuracy better than a degree. Two fringe patterns are formed after the oppositely traveling beams are recombined at the beamsplitter B. (See Fig. 16). Beamsplitter A makes the second fringe pattern easily observable by deflecting it away from the light source. Using an HeNe laser makes it difficult to eliminate a weak Fabry-Perot fringe pattern formed by the laser output mirror, the beamsplitter B and the fiber. This fringe pattern is fiber temperature dependent and produces an apparent fringe shift noise equivalent to 10^{-3} fringes or more. A diode laser light source makes the finesse of this Fabry-Perot interferometer so small that the corresponding noise is unobservable (less than 10^{-6} of the main Sagnac fringe shift readout). Another potential Fabry-Perot fringe pattern, formed by the fiber ends, was eliminated by cutting the fiber ends at about 10° angle with respect to the plane perpendicular to the fiber axis. The measured beam power at the fringe patterns is about 10 μW.

Fig. 16 Picture of the apparatus assembled as in Fig. 15.

The photon noise equivalent fringe shift ΔZ_n is

$$\Delta Z_n = \frac{1}{2\pi}\sqrt{\frac{1}{N}} \text{ fringes} \tag{25}$$

where N is the number of photons detected in an observation time interval.

Another form of this equation is

$$\Delta Z_n = \frac{\sqrt{B}}{2\pi}\sqrt{\frac{h\nu}{\eta P}} \tag{26}$$

where B is the detector bandwidth, $h\nu$ is the energy per photon, η is the photodetector efficiency, and P is the beam power at the photodetectors. The observation time $t = \frac{1}{B}$ and $N = \frac{\eta P t}{h\nu}$. In this case, $P = 10\ \mu W$, $\eta = 0.5$, and $t = 0.2$ s. Hence, the photon noise limited fringe shift ΔZ_n is $\Delta Z_n \cong 10^{-7}$ fringes. The fringe shift ΔZ in a fiber zyro is given by

$$\Delta Z = \frac{2\omega LR}{\lambda c} \tag{27}$$

here ω is the angular velocity, L is the fiber length, R is the fiber coil radius, λ is the free space wavelength of light, and c is the free space velocity of light.

The fringe shift measurement consists of detecting photocurrent changes at the complementary fringe patterns.

To maximize the photocurrent variation with ω, the circular fringes were made large (compared with the gaussian intensity distribution of the beam) such that all photons in the (complementary) fringe patterns fall on the photodetectors. The photocurrent difference was recorded.

In an ideal, perfectly adjusted Sagnac interferometer, the center of the fringes that appears in the direction of the light source would have the maximum intensity for zero angular velocity. The complementary fringe would have minimum intensity. This would make the instrument sensitivity zero for $\omega = 0$. To bias the interferometer, one can make the beam path external to the fiber nonreciprocal by slight, deliberate misalignment of the fiber ends. It is possible to reach a 90° bias this way, but at the expense of considerable beam power. The use of metallic beamsplitters also produces a biasing fringe shift because of the phase shift for nonperpendicular metallic reflection. The loss in this case is only about 30% per reflection. The phase bias in this experiment was about 50°. The sensitivity of this gyroscope is ($L = 620$ cm, $R = 17$ cm, $\lambda = 8.5 \times 10^{-5}$ cm) $\frac{\Delta Z}{\omega} = 1.5 \times 10^{-4}$ fringes/deg/s $= 8.6 \times 10^{-3}$ fringes/rad/s. Figure 17 shows a recording of the gyroscope output as the angular velocity of the rate table is changed with steps of one degree/s. The signal-to-noise ratio is about 4, making the smallest observable angular velocity change $\delta\omega = 0.3$ deg/s. This corresponds to fringe shift uncertainty $\delta(\Delta Z) = 3 \times 10^{-5}$ fringes: about 50 times the fringe shift produced by the earth rotation rate ($\omega_e = 7 \times 10^{-5}$ rad/s). Most of the observed slow drift

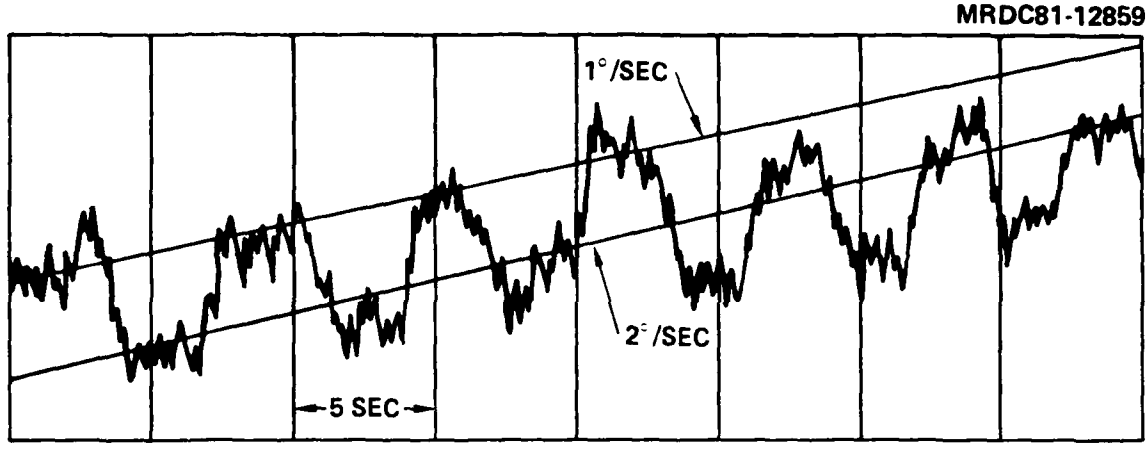

Fig. 17 Output signal from fiber gyro with polarization maintaining fiber.

and noise are attributed to relative interferometer component motion and is therefore independent of the fiber length. All the interferometer components are mounted rigidly within the 17 cm radius fiber coil with fiber holders about 7 cm from the axis of rotation. However, the centrifugal force generated by 1 rad/s rotation was sufficient to produce photocurrent change equivalent to about half of the Sagnac effect fringe shift. This effect is easily verified because it is independent of rotation direction. Figure 18 shows a recording of the gyro output with sinusoidally varying angular velocity with the trace repeated three times; the upper three (almost over lapping) traces are the output of the Sagnac gyro. Variations amounted to about one tenth of the amplitude.

The angular velocity amplitude was ω_{max} = 0.035 rad/s. making the noise limited rotation rate uncertainty $\delta(\omega)$ = 0.0035 rad/s. Therefore, with this fiber gyro (L = 6.2 meters), the smallest detectable rotation rate is a factor of 50 larger than the earth angular velocity. The increase of fiber length increases the gyro sensitivity without increasing the component motion noise.

These measurements show that the reflection noise can be reduced to levels where fringe shifts of 10^{-6} fringes or less can be detected. In addition, for a 6.2 meter long fiber, the polarization noise is considerably below the present largest noise source - the component motion.

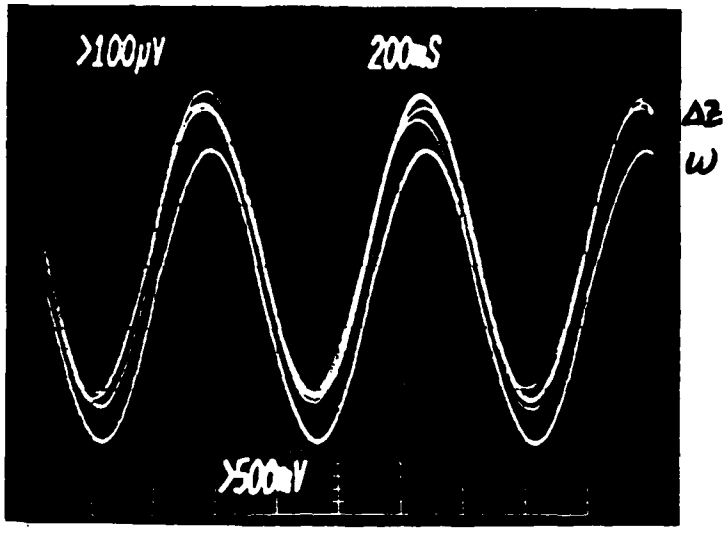

Fig. 18 Gyro output voltage with sinusoidally varying angular velocity.

4.0 CONCLUSIONS AND RECOMMENDATION

These recent experiments at Rockwell indicate that the polarization noise is reduced drastically when polarization maintaining fibers are used. This leaves the component (the interferometer parts - beamsplitters, lenses, etc.) motion as the next largest noise source.

The changes in component positions (that produce the changeable non-reciprocity and therefore fringe motion) can be reduced by the use of very small components and rigid mounting procedures. However, some thermal and acoustic sensitivity remains.

It is therefore suggested that all of the beam path that forms the interference pattern be confined in the same polarization maintaining fiber. It involves etching a few centimeters length of fiber almost down to the core and placing the fibers in contact with each other in an index matching substance. The distance between the cores and the contact length determine the power division. This can be done using fiber beamsplitters. Single-mode fiber-optic power dividers have been made. No effort has been made, however, to maintain polarization in these devices.

In case of stressed high birefringence polarization maintaining fibers (similar to the Bell fiber),[22] the etching technique developed by Sheem and Giallorenzi[21] cannot be used because the outer jacketing that stresses the fiber (and makes it polarization maintaining) is entirely removed. Another technique for making fiber beamsplitters was developed by Shaw.[23,24] The

fiber is polished flat on one side down to the core. Two of these fibers are then placed parallel with the polished, flat surfaces touching. The relative core alignment (angular with respect to the fiber azes directions, and lateral) determines the power division between the fibers).

Two different techniques are suggested for making polarization maintaining beamsplitters.

1. Polishing the fiber ends at 45° angle with respect to the fiber axes, then evaporating a half reflecting surface on the end (one fiber) and fastening (glueing) two such fiber ends together such that they form a 90° angle. This is the fiber analogue of a bulk optical beamsplitter.

2. Using a polarization maintaining fiber that relies on core ellipticity (and high index difference). This fiber has been made.[25] In this case, a technique similar to Shaw's can be used.

Figure 19 shows the intended configuration of the fiber ends for the stress birefringent polarization maintaining fibers. Light from the laser is focussed to the area where the two fiber cores touch at 45° angle. One of the fiber ends is made 50% reflecting. Light is divided into two equal intensity beams by this beamsplitter. If the ends are immersed in an index matching substance (that matches the cladding index), no special optics (or procedure)

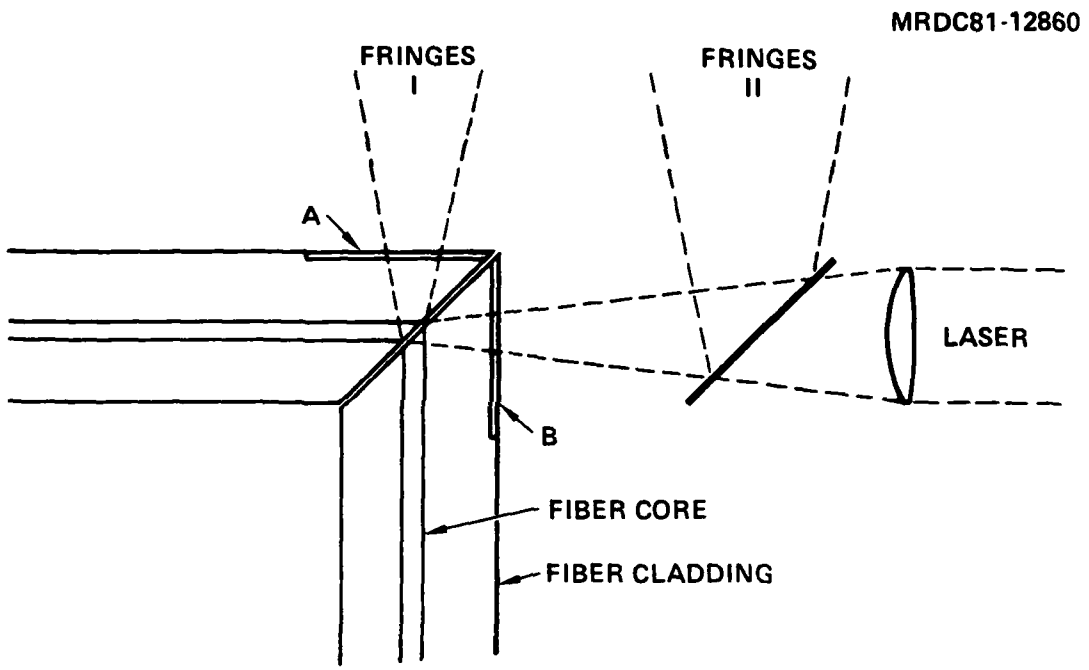

Fig. 19 Beam splitter configuration for ultra stable gyro.

is required for beam focusing. However, if there is an air path between the light source and the beamsplitter, surfaces A and B have to be polished flat. An external beamsplitter is required to see the complementary fringe pattern.

It is to be noticed that the fringe "pattern" in this case is only the center part of the typical fiber interferometer "bull's-eye" type fringes. The measurement, therefore, amounts to determining the light intensity variations at I and II. The amount of stress pattern distortions in the fiber due to the 45° cut at the fiber end is tolerable. Our experience with a Bell fiber that has $\Delta n = 2 \times 10^{-5}$ (beat length 3.3 cm) indicates that glueing such a fiber over a length of one millimeter or less does not introduce noticeable polarization scrambling.

The Andrew Corporation polarization maintaining fiber[25] relies on the core ellipticity (a/b = 2.5) and a high index difference between core and cladding ($\Delta n = 0.065$) to produce very short beat length. Here the effective index difference between the two polarizations is between 10^{-4} and 10^{-3}.

In this case, the Shaw technique can be used. There is the additional requirement that the polishing off of one side of the fiber has to be done on the fast or the slow axes with accuracy better than 2°.

Both of these suggestions should be studied experimentally. The techniques of fiber preparation are quite similar and require about the same type of laboratory equipment. The polarization maintaining fibers are not yet commercially available. Andrew Corporation plans to start selling their fiber

in the near future. ITT has recently obtained a contract from NRL to produce stress birefringent polarization maintaining fibers similar to Bell Labs fiber. Their delivery date has not been set.

5.0 RECOMMENDATION

The experimental results of this study confirmed the belief that for any phase sensitive fiber optic sensor a polarization maintaining fiber or a mechanism for creating one must be present. Since most of the mechanical or electro-mechanical techniques for inducing constant polarization in fibers are neither practical or effective for long fibers the answer ultimately lies in developing long lengths of single mode polarization maintaining fibers. Considerable effort should be expended to develop such fibers as they do not now exist in the quantity or lengths required for many applications. Until such fibers are available, engineering efforts for fiber gyros, etc., will show little payoff.

6.0 REFERENCES

1. V. Vali and R.W. Shorthill, "Fiber Ring Interferometer," Appl. Opt., 15, p. 1099-1100, May 1976.

2. V. Vali and R.W. Shorthill, "Ring Interferometer 950 m Long," Appl. Opt., 16, p. 290-291, Feb. 1977.

3. V. Vali, R.W. Shorthill, and M.F. Berg, "Fresnel-Fizean Effect in a Rotating Optical Fiber Ring Interferometer," Appl. Opt. 16, p. 2605-2607, Oct. 1977.

4. M.N. McLandrich and H.E. Rast, "Fiber Interferometer Gyroscope," SPIE Technical Symposium, San Diego, CA, Aug. 1978.

5. D.E. Thompson, D.B. Anderson, S.K. Yao, and B.R. Youmans, "Sagnac Fiber-Ring Gyro With Electronic Phase Sensing Using a (GaAl)As Laser," Appl. Phys. Lett., 33, p. 940-941, Dec. 1, 1978.

6. R.F. Cahill and E. Udd, "Phase-nulling Fiber Optic Laser Gyro," Opt. Lett, 4, p. 93-95, March 1979.

7. J.A. Bucaro, H.O. Dardy, and E.F. Carome, "Optical Fiber Acoustic Sensor," Appl. Opt., 16, p. 1761-1765, July 1977.

8. J.A. Bucaro, H.O. Dardy, and E.F. Carome, "Fiber-optic Hydrophone," J. Acoust. Soc. Am., 62, p. 1302-1308, Nov. 1977.

9. J.H. Cole, R.L. Johnson, and P.G. Bhuta, "Fiber-Optic Detection of Sound," J. Acoust. Soc. Am., 62, p. 1136-1138, Nov. 1977.

10. J.A. Bucaro and E.F. Carome, "Single Fiber Interferometric Acoustic Sensor," Appl. Opt., 17, p. 330-331, Feb. 1, 1978.

11. B. Calshaw, D.E.N. Davies, and S.A. Kingsley, "Acoustic Sensitivity of Optical Fiber Waveguides," Electron. Lett, 13, p. 760-761, Dec. 8, 1977.

12. M.R. Layton and J.A. Bucaro, "Optical Fiber Acoustic Sensor Utilizing Mode-Mode Interference," Appl. Opt., 18, p. 666-670, March 1, 1979.

13. J.A. Bucaro and T.R. Hickman, "Measurement of Sensitivity of Optical Fibers for Acoustic Detection," Appl. Opt., 18, p. 938-940, March 15, 1979.

14. A.M. Smith, "Polarization and Magnetooptic Properties of Single-Mode Optical Fiber," Appl. Opt., 17, p. S2-S6, Jan. 1, 1978.

15. R.C. Rashleigh and R. Ulrich, "Magneto-optic Current Sensing with Birefringent Fibers," Appl. Phys. Lett., 34, p. 768-770, June 1, 1978.

16. G. Schiffner, W.R. Leeb, H. Krammer, and J. Wittmann, "Reciprocity of Birefringent Single-Mode Fibers for Optical Gyros," Appl. Opt., 18, p. 2096-2097, July 1, 1979.

17. R. Ulrich and M. Johnson, "Fiber-ring Interferometer: Polarization Analysis," Opt. Lett., 4, p. 152-154, May 1979.

18. V. Vali and M. F. Berg, "Nonreciprocity Noise in Fiber Gyroscopes and Measurement of Fiber Dispersion," SPEE, San Diego, August 1978.

19. S.-C. Lin and T.G. Giallorenzi, "Sensitivity Analysis of the Sagnac-Effect Optical-Fiber Ring Interferometer," Appl. Opt., 18, p. 915-931, March 15, 1979.

20. R. Ulrich and A. Simon, Applied Optics, 1 July 1979, 18, No. 13, p. 2241.

21. S. K. Sheem and T. G. Gaillorenzi, "Single-mode Fiber-optical Power Divider: Encapsulated Etching Technique," Opt. Lett. 4, No. 1, p. 29, Jan. 1979.

22. R. H. Stolen, V. Ramaswamy, P. Kaiser, and W. Pleibel, "Linear Polarization in Birefringent Single-mode Fibers," Appl. Phys. Lett., 33, No. 8, p. 699, 15 Oct. 1978.

23. M. McLandrich, FOSS Workshop, 12-14 December 1979, NRL, Washington, D.C.

24. J. Shaw, FOSS Workshop, 12-14 December 1979, NRL, Washington, D.C.

25. R. B. Dyott, J. R. Cosens and D. G. Morris, "Preservation of Polarization on Optical-fiber Waveguides with Elliptical Cores," Electron. Lett., 15, No. 13, 21 June 1979.

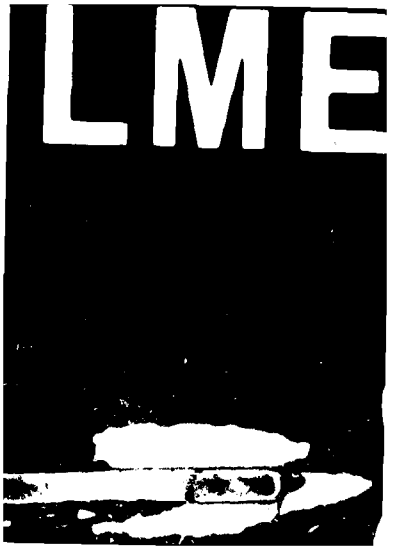
LME